

Vaughan, Wareham and Millar

**Granitoid pluton formation by spreading of continental crust: the Wiley
Glacier complex, northwest Palmer Land, Antarctica.**

ALAN P.M. VAUGHAN¹, CHRISTOPHER D. WAREHAM¹ AND IAN L. MILLAR²

¹British Antarctic Survey, High Cross, Madingley Rd., Cambridge CB3 0ET, UK.

*²British Antarctic Survey, c/o NERC Isotope Geosciences Laboratory, Keyworth, Nottingham,
NG12 5GG, UK.*

A.P.M. Vaughan:

e-mail: a.vaughan@bas.ac.uk

Fax: +44+1223+362616

C. D. Wareham:

e-mail: c.wareham@bas.ac.uk

Fax: +44+1223+362616

I.L. Millar:

e-mail: i.millar@bas.ac.uk

Fax: +44+115+9363302

Please address all correspondence to Alan Vaughan at address 1

Abstract

The emplacement mechanism, geometry, and isotope geochemistry of plutons of the Wiley Glacier complex suggest that new continental crust grew by multiple injection of tonalitic dykes during dextral transtension in the Antarctic Peninsula magmatic arc in Early Cretaceous times. The suggested mechanism is analogous to basalt dyke injection during sea-floor spreading. During normal-dextral shear, the Burns Bluff pluton, a sheeted, moderately east-dipping, syn-magmatically sheared tonalite–granodiorite intruded syn-magmatically sheared quartz diorite of the Creswick Gap pluton and 140 ± 5 Ma hornblende gabbro. U–Pb dating of zircon and Ar–Ar dating of hornblende and biotite suggest that both granite *s.l.* plutons were emplaced between 145 and 140 Ma, but that extensional shearing was active from the time of emplacement until *ca* 127 Ma. The Burns Bluff pluton is chilled at its margin, and grades through mylonitized, porphyritic tonalite–granodiorite sheets and tonalite–granodiorite sheets with minor chilling, to a km-scale body of coarse-grained, hypidiomorphic tonalite–granodiorite. Co-magmatic microdiorite forms dykes and abundant synplutonic mafic enclaves. These dykes opened as echelon veins during episodic dextral shear and were deformed to trains of enclaves during continued normal-dextral shear. Pluton-marginal porphyritic and hypidiomorphic tonalite–granodiorite forms large, fault-hosted sheets emplaced progressively under extension with minor dextral shear. Kinematic indicators from pluton-marginal granite *s.l.* dykes suggest that early in pluton accretion, intrusive sheets cooled rapidly, with simple shear prior to full crystallization changing to ductile simple shear during cooling. Kinematic indicators towards the pluton core suggest that as the pluton grew, and cooled more slowly, emplacement switched from sheeting to *in situ* inflation with simple shear distributed across a broad zone prior to full crystallization of magma. Cross-cutting relationships with the coeval, syn-extensional, Creswick Gap pluton

suggest that the Burns Bluff pluton was emplaced in a steeper, second generation shear structure, like those in normal fault systems. This suggests that the Wiley Glacier complex was emplaced above the base of the brittle–ductile transition zone (15–18 km depth). The Burns Bluff pluton has Nd and Sr isotope values that range from mantle dominated ($\epsilon\text{Nd}_{141} = +3.8$, $^{87}\text{Sr}/^{86}\text{Sr}_{141} = 0.70468$) to more crustally influenced ($\epsilon\text{Nd}_{141} = -1.7$, $^{87}\text{Sr}/^{86}\text{Sr}_{141} = 0.70652$). This range probably represents different degrees of mixing between mantle-derived magma and lower crustal partial melts generated in the garnet-stability zone (40+ km depth). Addition of new crustal material by mafic underplating at the base of the crust and by redistribution of granitic *s.l.* and mafic, modified, underplated magma to mid-crustal levels along extensional shear zones as the arc “spread” were the primary mechanisms of crustal growth.

Keywords: diapir, adakite, Gondwana, Pacific

1. Introduction

Mechanisms of granite magma transport and pluton formation are the subject of vigorous debate (see Pitcher, 1993, Chapter 11, for discussion), and are critical to understanding the formation of continental crust. Continental crust may grow magmatically by addition of juvenile, mantle-derived, mafic magma to the lower crust. New mafic material added to the base of the crust is vulnerable to loss by delamination, so further processes are necessary for net crustal growth. Key to these processes is the genesis and emplacement of granite magma. Granite magma is a likely product where previously accreted mantle magma is remelted or newly accreted mantle magma is fractionated. Net addition to the continental crust will result if mantle-derived, mafic or granite *s.l.* magma is redistributed to the middle or upper crust where delamination does not occur.

Although granite may be emplaced under many stress regimes, extensional models for granite emplacement (e.g. Hutton et al., 1990; Hutton, 1992; Petford et al., 1993; Grocott et al., 1994) have been proposed as good solutions to the problem of how space in the crust is made for granites, the so-called granite “room” problem (Paterson and Fowler, 1993). Nevertheless, Paterson and Fowler (1993) pointed out that the space made in this way must be compensated for by material-transfer in the crust or mantle. Detailed structural and isotopic analysis presented here of the Creswick Gap and Burns Bluff plutons, kinematically layered trondhjemite–tonalite–granodiorite (TTG) plutons of the Wiley Glacier complex from the Antarctic Peninsula, sheds light on some aspects of granite emplacement under extension. Here, we propose that far-field extension of the arc, driven by pull of subducting slab and rolling back of the hinge (driven by sinking of oceanic lithosphere into the mantle; in this case the compensatory material transfer process required by Paterson and Fowler (1993)), produced near-field extension on shear zones and thus room for the plutons of the Wiley Glacier complex. This paper presents (1) evidence for granite emplacement in a developing system of normal-dextral-sense shear zones by a mechanism normally associated with basalt dyke injection and spreading at mid-ocean ridges, and (2) isotopic analysis of the Wiley Glacier complex that suggests its emplacement represents net growth of continental crust.

2. Geological setting

From at least the Middle Triassic to Early Tertiary, the Antarctic Peninsula formed part of an arc that extended from southern South America to pre-rift New Zealand (Fig. 1) (Storey et al., 1996). The peninsula comprises arc magmatic rocks and Triassic, or older, basement rocks, with minor volcanic and sedimentary components. Arc magmatism was

particularly voluminous in the Early Cretaceous, much of it coeval with crustal extension (Vaughan and Millar, 1996); Figure 2 shows crustal-scale, extensional shear zones in northwest Palmer Land that hosted a suite of mafic and TTG plutons, ranging from hornblende gabbro to leucogranite, between 140 and 110 Ma.

The Wiley Glacier complex forms a geologically contiguous massif between Creswick Gap and George VI Sound (Figs 2 & 3). It comprises, from north to south, Renner Peak, Burns Bluff, Creswick Peaks and Moore Point (Fig. 3). Although Harrison (1989) recorded bosses of layered, quartzofeldspathic gneiss (e.g. at Burns Bluff, Fig. 3), similar to Upper Triassic–Lower Jurassic gneiss from elsewhere in Palmer Land (Piercy and Harrison, 1991), we did not examine these in detail. East to west, the massif comprises plutons of Creswick Gap granodiorite–quartz diorite, Burns Bluff tonalite–granodiorite and Moore Point hornblende gabbro. Igneous contacts and plutons strike roughly east-southeast and dip moderately east.

2.1. Creswick Gap pluton

The Creswick Gap pluton forms the eastern parts of Creswick Peaks, Burns Bluff and Renner Peak. It comprises mainly granodiorite but ranges from quartz diorite to granodiorite. Granodiorite of the Creswick Gap pluton at Creswick Peaks has a U–Pb zircon age of 141 ± 2 Ma (Vaughan and Millar, 1996). Sheared Creswick Gap granodiorite and quartz diorite form the eastern (hanging-wall) and western (footwall) wall rock of the Burns Bluff pluton respectively. Hornblende from extensional mylonite of the Creswick Gap granodiorite has given a K–Ar age of 140 ± 4 Ma (Vaughan and Millar, 1996).

Quartz diorite

The quartz diorite comprises a hypidiomorphic assemblage of poikilitic hornblende (0.4–3 mm) with chadacrysts of opaques, plagioclase and prismatic apatite; partially sericitized, concentrically-zoned andesine (An₃₄–An₄₉) and replacive albite (0.2–4.3 mm); quartz (0.04–0.6 mm); relict clinopyroxene in hornblende (0.08–0.2 mm); and biotite and chlorite (0.08–0.8 mm). Accessories include opaque grains (probable titanomagnetite), titanite, prismatic apatite, monazite, and zircon.

Granodiorite

The granodiorite comprises a hypidiomorphic assemblage of 40–60% andesine (An₃₆–An₄₅, 0.08–3.2 mm); weakly poikilitic hornblende (0.08–3 mm) with chadacrysts of opaque grains and apatite; quartz (0.1–0.4 mm), K-feldspar (0.04–0.1 mm) (*ca* 7%), and biotite (0.2–1.4 mm). Accessories include opaque grains, titanite and prismatic apatite.

2.2. Moore Point gabbro

Moore Point hornblende gabbro forms the southwestern corner of the Wiley Glacier complex. It also cuts granodiorite of the Creswick Gap pluton at east Burns Bluff. Moore Point gabbro, with Creswick Gap quartz diorite, forms the wall rock (footwall) west of the Burns Bluff pluton. Aplites that cut the gabbro have been dated at 140 ± 5 Ma by the Rb–Sr whole rock method (Piercy and Harrison, 1991).

Hornblende gabbro

The hornblende gabbro comprises a hypidiomorphic assemblage of poikilitic hornblende (0.1–1.5 mm) with chadacrysts of prismatic apatite and feldspar; partially sericitized, concentrically-zoned labradorite (An_{51} – An_{62} , 0.25–7 mm) with andesine rims (An_{34}); and secondary chlorite (0.2–0.5 mm). Accessory opaque grains (0.05–0.35 mm), with brown alteration rims, are abundant. Prismatic apatite is abundant, interpenetrating with hornblende.

2.3. Burns Bluff pluton

The sheet-like Burns Bluff pluton crops out at western Burns Bluff and Creswick Peaks. It cuts the Creswick Gap pluton and Moore Point gabbro. From north-northwest–south-southeast it tapers from over 1 km wide to *ca* 30 m. Its core is hypidiomorphic tonalite–granodiorite, with a western zone of mylonite, sheets of porphyritic tonalite–granodiorite, hypidiomorphic tonalite–granodiorite, aplite and microdiorite. Primary, compositional layering is a distinctive feature of the Burns Bluff pluton.

Porphyritic tonalite–granodiorite

This comprises a porphyritic to mylonitic assemblage of partially sericitized, concentrically-zoned seriate andesine (An_{31} , 1–5 mm); quartz (0.008–0.12 mm); planar aggregates of secondary biotite (aggregates 20 x 5 x 1 mm, subgrains 0.02–0.2 mm) after hornblende; and perthitic K-feldspar (0.8–1.8 mm). Accessories include opaque grains, chlorite, zircon, and prismatic apatite.

Aplite

The aplite is a sub-hypidiomorphic to mylonitic assemblage of perthite (0.4–3.5 mm); sericitized andesine (An₃₄–An₄₀, 0.25–3 mm); quartz (0.01–0.4 mm); and biotite (0.02–0.2 mm), with accessory, epidote, titanite, hornblende, garnet, chlorite, and opaque grains.

Tonalite–granodiorite

This comprises a sub-hypidiomorphic assemblage of partially sericitized, weakly poikilitic, concentrically-zoned plagioclase with oligoclase–andesine (An₂₆–An₃₆) cores, oligoclase (An₂₀) rims, hornblende chadacrysts, and replacive albite (1.2–4 mm); quartz (0.03–0.3 mm), poikilitic hornblende (0.25–3 mm) with chadacrysts of plagioclase and prismatic apatite; and biotite (0.05–0.2 mm). Accessories include opaque grains, rutile, and zircon.

Microdiorite

This forms dykes and synplutonic xenoliths and comprises a hypidiomorphic to porphyritic assemblage of partially sericitized, concentrically-zoned andesine and replacive albite (An₃₅–An₄₀, framework grains 0.16–1 mm, porphyroclasts/phenocrysts 1.4–4 mm); 25–40%, weakly poikilitic hornblende (0.04–2 mm) with chadacrysts of opaques and prismatic apatite; and opaque grains (probably magnetite, 0.02–2.4 mm). Accessories include biotite, prismatic apatite, titanite, and epidote.

3. Geochronology

Five zircon fractions of the Creswick Gap pluton at Renner Peak and at Burns Bluff, and two fractions of the Burns Bluff pluton tonalite–granodiorite were analysed using the U–Pb method (Table 1). Two samples of sheared Creswick Gap pluton at Creswick Peaks were analysed using Ar–Ar laserprobe dating (Table 2).

3.1. Creswick Gap pluton

The zircon data from the Creswick Gap pluton plot close to the data of Vaughan and Millar (1996), but are slightly discordant, suggesting a small inherited component (quartz diorite at Burns Bluff, Figure 4a; granodiorite at Renner Peak, Figure 4b). The zircons lie too close to concordia to allow determination of a meaningful upper intercept age for the inherited component. However, the data are consistent with inheritance of zircons from northwestern Palmer Land Triassic basement gneisses, which themselves contain considerable Proterozoic–Palaeozoic inheritance. The discordant Creswick Gap pluton zircons have very low Pb concentrations (*ca* 2 ppm) compared to Triassic gneisses (*ca* 40–70 ppm) and very little inherited Triassic zircon would be needed to cause the degree of discordance shown by the Creswick Gap pluton zircons. However, discordance may also be a product of Pb-loss.

Biotite and hornblende samples from relatively undeformed Creswick Gap granodiorite at Creswick Peaks yielded ^{40}Ar – ^{39}Ar laserprobe method ages of 139.4 ± 2.4 Ma and 144.6 ± 3.6 Ma respectively (Figs 5a and 5b), which are within error of the U–Pb method age above. Amphibole samples from extensional ultramylonite zones in Creswick Gap granodiorite at Creswick Peaks yielded an ^{40}Ar – ^{39}Ar laserprobe method age of $127.1 \pm$

2.5 Ma (Fig. 5c).

The zircon age from the Creswick Gap pluton and the ^{40}Ar – ^{39}Ar ages from the relatively undeformed granodiorite overlap within analytical error. The weighted mean of the three ages is 141 ± 2 Ma. However, it is conceivable that the near-concordant zircon analyses from the Creswick Gap pluton have suffered a small degree of recent Pb-loss: the $^{207}\text{Pb}/^{206}\text{Pb}$ model ages of the three most concordant points range from 142–148 Ma (Vaughan and Millar, 1996). It is therefore possible that the older ^{40}Ar – ^{39}Ar age of 144.6 ± 3.6 Ma represents the true emplacement age of the pluton. Combining the data, it seems reasonable to suggest that the Creswick Gap pluton was emplaced between 145 and 140 Ma.

3.2. Burns Bluff pluton

Two zircon fractions of the Burns Bluff tonalite–granodiorite were analysed (Table 1, Figure 4a). Cross-cutting relationships indicate that the tonalite–granodiorite must be younger than the Creswick gap pluton. One analysis plots close to the data for quartz diorite of the Creswick Gap host pluton. This zircon fraction must therefore contain an inherited component. The second analysis has relatively high common Pb, and gives an imprecise determination, overlapping concordia at around 136 Ma. This is consistent with recent lead-loss from *ca* 140 Ma zircons. Given this limited data set, it is not possible to give a precise age determination for Burns Bluff pluton, although the data are compatible with emplacement of the tonalite–granodiorite soon after the Creswick Gap pluton.

4. Structure

The structural and temporal relationships of the magmatic components of the Wiley

Glacier complex are well exposed at western Burns Bluff (Fig. 3) and this area was studied in detail. The rocks are described below from west to east, and oldest to youngest. The data collected focus on the geometries of fabrics, their relative ages, the orientation of tectonic lineations, the shear sense of kinematic indicators, and the timing of fabric development relative to magmatic crystallization. We use the terminology of Hutton (1988) and refer to magmatic-state structures and deformation as pre-full crystallization (PFC).

Western Burns Bluff comprises a contact zone between sheared and mylonitized Burns Bluff tonalite–granodiorite, and deformed Creswick Gap quartz diorite and Moore Point hornblende gabbro. Dykes of Burns Bluff tonalite–granodiorite form a broad, 50- to 100-m-wide zone that dips moderately east to southeast and forms the west margin of the Burns Bluff pluton. In this contact zone, Burns Bluff tonalite–granodiorite is intercalated with selvages of Creswick Gap quartz diorite and Moore Point hornblende gabbro up to 13 m thick. Sheets 1.5–13.5 m thick of Burns Bluff hypidiomorphic and porphyritic tonalite–granodiorite, aplite, and microdiorite are abundant. Eastwards from the marginal zone, the Burns Bluff pluton shows a transition from sheets of intrusion-marginal, chilled and mylonitized tonalite–granodiorite to weakly deformed tonalite–granodiorite of the pluton core (Fig. 6a). A 50 m section of the eastern part of the marginal zone margin was logged in detail. Where it was logged, it comprises selvages of quartz diorite and hornblende gabbro, and dykes of hypidiomorphic and porphyritic tonalite–granodiorite, and aplite (Fig. 7). All lithologies show syn-magmatic and high-temperature-ductile structures, including mylonite, that formed during extensional simple shear.

4.1. Creswick Gap quartz diorite and Moore Point hornblende gabbro

An earlier history of synmagmatic deformation is preserved in the thick selvages of Creswick Gap quartz diorite and Moore Point hornblende gabbro that are intercalated with the Burns Bluff pluton on its western margin. Much hornblende is curved, with asymmetric, σ - and δ -porphyroblast-like (Passchier and Simpson, 1986), and “mica-fish”-like, shapes (Fig. 8a). Feldspar phenocrysts are tiled with a consistent sense (Fig. 8b). Plagioclase is curved and fractured and pericline twinning appears mechanically-induced. Fine-grained quartz forms interconnected blebs and ribbons that mantle hornblende and feldspar augens. Where hornblende grain-shape is highly irregular, biotite and chlorite form tails on hornblende porphyroblasts (deformation appears to have been more ductile than magmatic in these areas). Opaque grains have elongate, anastomosing shapes, and mantle feldspar and hornblende augens. In some cases they have σ -porphyroblast-like shapes, and appear to have been ductilely deformed. Some apatite prisms are curved. Hornblende and feldspar define a composite fabric (S_1) comprising a grain-long-axis preferred-orientation fabric and an anastomosing grain-boundary preferred-orientation fabric that dips moderately to steeply north (Fig. 9a) with a mineral stretching lineation (L_1) defined primarily by hornblende. The foliation is openly folded (F_1) with interlimb angles of 130° – 150° . The axial planes of these folds dip moderately to steeply south and the folds plunge shallowly east, similar to syn-extensional folds described from the Creswick Gap pluton at Creswick Peaks (Vaughan and Millar, 1996). Long axes of quartz blebs, opaque grains and phyllosilicate grains are sub-parallel to the anastomosing component of the fabric. The sense of vorticity of hornblende δ -porphyroblasts and the sense of asymmetry of “hornblende-fish” suggest deformation during normal-sense shear under PFC to ductile conditions, but with temperatures above 800°C , the brittle–ductile transition for hornblende (Rooney et al., 1975).

4.2. Western limit of contact zone

At the farthest southwest exposure of the Burns Bluff pluton, quartz diorite of the Creswick Gap pluton is in sheared contact with a 20 m-thick, syn-magmatically sheared, porphyritic, tonalite–granodiorite unit. The contact zone between porphyritic tonalite–granodiorite and quartz diorite dips steeply east. Sheared laminar quartz veins, approximately 5 cm wide, similar to bedding-parallel detachment veins (Fitches et al., 1986) mark the contact. The presence of veins of this type suggests that multiple brittle–ductile re-activations of the contact zone have occurred.

4.3. Burns Bluff porphyritic tonalite–granodiorite

Feldspar in Burns Bluff porphyritic tonalite–granodiorite is “tiled” (Fig. 8c) (Paterson et al., 1989) with a consistent sense. Lamellar twins in plagioclase are curved with sweeping extinction and pericline twinning appears mechanically-induced. Hornblende is curved with sweeping extinction. Fine-grained quartz forms elongate aggregates, with mortar texture and S–C mylonite fabrics. Biotite, in one case, shows internal Riedel veins of chlorite where crystallographic planes have separated perpendicular to 001. In zones of high shear strain (ultramylonite), defined by quartz low grain-size and strongly developed feldspar augens draped by quartz ribbons, tiled feldspar is modified to σ_a -porphyroclasts (Fig. 8d). Feldspar porphyroclasts, quartz ribbons and biotite aggregates define a strong grain-long-axis and grain-boundary preferred-orientation fabric. Sense-of-imbrication of tiled feldspar phenocrysts, curvature of S–C surfaces and sense of vorticity of feldspar porphyroclasts suggest uniform normal-sense shear.

4.4. Burns Bluff aplite

Aplite units are generally mylonitized with mortar-texture developed in quartz and feldspar. Feldspar is commonly rhombic in section, and forms predominantly σ_a -type porphyroclasts, although δ - and overturned-types are also evident. Quartz-strings mantle feldspar porphyroclasts, and in some cases form tails. Lamellar twins in andesine are curved with sweeping extinction, and in K-feldspar, perthite and grain-boundary myrmekite all appear mechanically-induced. Plagioclase defines a moderate grain-long-axis preferred-orientation fabric. Quartz and perthite define a strong grain-long-axis and grain-boundary preferred-orientation fabric. Titanite and deformed hornblende are aligned with grain long-axes sub-parallel to the quartz-perthite fabric. The sense of vorticity of feldspar porphyroclasts suggests deformation during ductile normal shear.

4.5. Burns Bluff hypidiomorphic tonalite–granodiorite

In sheets of hypidiomorphic Burns Bluff tonalite–granodiorite, hornblende and plagioclase are “tiled” (Fig. 8e) (Paterson et al., 1989). Lamellar twins in plagioclase are curved with sweeping extinction and pericline twinning appears mechanically-induced. Large, euhedral plagioclase phenocrysts show evidence of brittle–ductile fracture: transverse cracks are filled with fine-grained (0.1 mm) subhedral quartz and hornblende (Fig. 8f). This resembles “frozen” silicic melt and is contiguous with groundmass areas of similar mineralogy and form. Quartz generally forms fine-grained, elongate aggregates, and appears blastomylonitic. Biotite is asymmetric and curved with mica-fish-like geometries, and is associated with narrow zones of reduced grain-size of feldspar and hornblende. These zones contain concentrically-zoned oligoclase porphyroclasts, and resemble protomylonite, or “frozen” melt described above. Hornblende and feldspar define a moderate composite fabric

(S₂) comprising a grain-long-axis preferred-orientation fabric and a grain-boundary preferred orientation fabric with biotite. Quartz subgrains are elongate in areas of lower grain-size. They define a grain-long-axis and grain-boundary preferred-orientation fabric subparallel to that defined by plagioclase and hornblende. The hornblende–plagioclase–biotite–quartz foliation dips moderately to steeply northeast to southeast (Fig. 9b), with a mineral stretching lineation defined by hornblende and plagioclase (L₂). Xenoliths of microdiorite generally have long axes parallel to the foliation defined by feldspar and hornblende, and asymmetric geometries (Fig. 6b). The sense of imbrication of feldspar and hornblende, sense of asymmetry of synplutonic xenoliths, and the sense of dragging of curved biotite suggests deformation and grain-rotation during normal-dextral-sense simple-shear. Melt-injected, fractured plagioclase and ductilely deformed (curved) hornblende suggest that hot (> 800°C), crystallizing magma was first deformed pre-full crystallization and then ductilely deformed as it cooled.

4.6. Burns Bluff microdiorite dykes and enclaves

Weakly-chilled, microdiorite dykes, 1–3 m wide, with strikes clockwise to S₂, intruded Burns Bluff tonalite–granodiorite. Some dykes have extremely irregular geometries with cusped and lobate margins that show little evidence of chilling. Dykes can be traced laterally into zones of enclaves (Fig 10a), from which they are petrographically indistinguishable. Microdiorite enclaves are sub-spherical to asymmetric with uniform normal sense. In the main body of the pluton, where microdiorite dykes form continuous structures, they have undulose, slightly cusped margins, and form an echelon sets with zone-trend (the notional plane of simple shear in an echelon fissure systems, Rothery, 1988) dipping-moderately to -steeply southeast. Dyke terminations overlap with clockwise sense

and δ -angles (the angle between en echelon structures and the zone trend, Rothery, 1988) are approximately 10° (Fig. 11). δ -angles less than 45° indicate a component of extension to simple shear (negative dilation of Ramsay and Huber, 1983, pp 48–50) suggesting that the dykes were intruded under dextral transtension. However, the high δ -angle between the zone trend of the dyke arrays and the margin of the Burns Bluff pluton (Fig. 12) is more consistent with dykes opening during episodes of dextral shear. This suggests partitioning of dextral shear into the pluton core. In some cases microdiorite dykes contain xenoliths of coarse-grained quartz diorite similar to the host rock pluton. Fig. 10b summarizes the outcrop evidence of Fig. 10a, which suggests that microdiorite enclaves formed by deformation and disruption of synplutonic, microdiorite dykes during syn-magmatic simple shear. In the microdiorite dykes and enclaves, hornblende and plagioclase define a moderate grain-long-axis and grain-boundary preferred-orientation fabric. Hornblende is abundantly curved, with strongly sweeping extinction. Some lamellar twinning in plagioclase appears mechanically-induced and extinction is undulose. Although enclaves are asymmetric on a centimetre- to decimetre-scale no grain-imbrication is evident, and curved hornblende was deformed by pure shear. This may reflect higher viscosity or rapid chilling of microdiorite dykes or enclaves in tonalite–granodiorite undergoing simple shear.

5. Isotope geochemistry

Hypidiomorphic and porphyritic Burns Bluff tonalite–granodiorite were analysed for Nd and Sr isotopes to see if this shear-zone hosted pluton represented new continental crust. Gabbro from nearby Moore Point (Fig. 3), and hornblende gabbro and Creswick Gap quartz diorite forming the wallrock at Burns Bluff were also analysed to see if similar magmas were involved in the genesis of the Burns Bluff tonalite–granodiorite.

Gabbro at Moore Point, and hornblende gabbro and Creswick Gap quartz diorite at Burns Bluff have ϵNd_{141} between +2.6 and +4.3, $^{87}\text{Sr}/^{86}\text{Sr}_{141} < 0.7045$ (Table 3, Fig. 13). Their contents of Ni (19 to 113 ppm), Cr (40 to 362 ppm) and MgO (3.7 to 9.3 wt.%), low $^{87}\text{Sr}/^{86}\text{Sr}_{141}$, relatively high ϵNd_{141} , and cumulate character of these intrusions suggests that they are fractionated mantle-derived magmas. Hornblende gabbro and quartz diorite wall rocks at Burns Bluff are chemically more fractionated than the Moore Point gabbro (e.g., 19 to 52 ppm Ni) and have slightly lower ϵNd_{141} and variable $^{87}\text{Sr}/^{86}\text{Sr}_{141}$. Although fractional crystallization may have been accompanied by some crustal assimilation, isotope data preclude a major component of basement gneiss to the hornblende gabbro and quartz diorite at Burns Bluff. Most basement in the Antarctic Peninsula has relatively low ϵNd_{141} (as low as -8) and $^{87}\text{Sr}/^{86}\text{Sr}_{141} > 0.707$ (Hole, 1986; Milne and Millar, 1989; Wever et al., 1995). Triassic gneiss near Creswick Gap has ϵNd_{141} and $^{87}\text{Sr}/^{86}\text{Sr}_{141}$ of -4.5 and *ca* 0.708 respectively. Because the gabbro and quartz diorite at Burns Bluff have lower Sr and Nd contents (Table 3) than the gneisses (Sr *ca* 600 ppm and Nd *ca* 25 ppm), their isotope compositions would be sensitive to crustal contamination.

Hypidiomorphic tonalite–granodiorite (sample R.6057.7), appears to have been produced by fractional crystallisation of gabbro–diorite magma. Chemically, it is the most fractionated component of the pluton that was analysed, with 75 wt.% SiO₂, 0.5 wt. % MgO and a pronounced negative Eu anomaly. Its ϵNd_{141} is within error of the gabbro at Moore Point and two of the hornblende gabbro and Creswick Gap quartz diorite wall rock selvages on the margin of the Burns Bluff tonalite–granodiorite (Table 3, Fig. 13), suggesting it was produced by fractionation of feldspar and amphibole from a gabbro–diorite magma.

The oldest phase of the Burns Bluff pluton, porphyritic tonalite–granodiorite (sample R.6057.16), has the lowest ϵNd_{141} (-1.7) and highest $^{87}\text{Sr}/^{86}\text{Sr}_{141}$ (0.70652), suggesting that it contains a relatively large component of basement gneiss. However, its Sr and Nd isotope compositions suggest that it is not solely a partial melt of exposed crust (Fig. 13). We suggest that this magma type was produced by mixing of hornblende gabbro and quartz diorite magma with crust.

The remaining tonalite–granodiorite units from the Burns Bluff pluton have Sr and Nd isotope compositions that fall between those of the units discussed above (Table 3, Fig. 13). ϵNd_{141} range from -0.7 to +1.6 and $^{87}\text{Sr}/^{86}\text{Sr}_{141}$ from 0.70540 to 0.70550. These data are broadly consistent with gabbro–diorite magmas that assimilated crust, or mixed to a varying degree with partial melts of crust during their emplacement and crystallisation.

6. Discussion

6.1. Overall geometry of pluton complex

The Burns Bluff pluton and the Creswick Gap pluton show similar syn-magmatic deformation: In both cases syn-magmatic structures dip easterly (Fig. 9) and kinematics are extensional. However, Burns Bluff tonalite–granodiorite dykes cross-cut syn-magmatic structures in the Creswick Gap pluton and dip more steeply (Fig. 6c), and the hornblende and plagioclase mineral lineation plunge of the older Creswick Gap pluton (L_1) strikes more southerly (Fig. 9). The overall shape of the Burns Bluff granodiorite intrusion can be simplified as a large, echelon, fault structure that opened under dextral transtensional stress (Fig. 12). Synplutonic, microdiorite dykes are analogous to subsidiary "third order" *en*

échelon veins (Hancock, 1972) that opened during episodic dextral shear, possibly partitioned into the pluton core, and were deformed to enclaves.

6.2. *Granite magma s.l. transport along shear zones*

Petford et al. (1993) were the first workers to discuss numerically the ascent of granitic melt in faults or shear zones. Their work and numerical modelling by Rubin (1995a) suggests that shear zones are good vehicles for granite magma *s.l.* transport; structural discontinuities such as shear zones, overcome the problem of crack initiation (N. Petford pers. comm. 1997) where they intersect source regions of relatively viscous granitic melts. In the absence of shear zones, modelling predicts that, close to the source region "tip-freezing" will halt granite dykes that propagate purely by magma-pressure-driven elastic widening (Rubin, 1995b). Escape is enhanced and the rate of transfer of granitic magma *s.l.* is substantially increased by the addition of a mingled component of lower viscosity mafic magma (Carrigan et al., 1992). Abundant enclaves of mingled mafic magma (Vaughan et al., 1995, Vaughan and Millar, 1996) provide circumstantial evidence that magma-mingling assisted the ascent of Wiley Glacier complex pluton magmas.

6.3. *Dyke-by-dyke pluton growth*

Channelling and freezing of granite magma in shear-zones, such as in an actively extending arc, favours formation of dyke-like bodies (Hutton, 1992) (e.g. Fig. 6a). The margin and shape of the Burns Bluff pluton (Figs 4a and 11), suggest that it grew initially by lateral accretion of metre-scale, tabular magma bodies. Kinematic indicators described above suggest that this was in a ductile extensional shear zone (Fig. 14a–d), a mechanism proposed

by Hutton (1992) and shown by numerical modelling to be feasible (Hanson and Glazner, 1995). Kinematic indicators that formed in crystal mushes under submagmatic conditions and in crystallized tonalite–granodiorite under ductile conditions indicate normal simple shear of cooling granitoid dykes at early stages in pluton accretion (Fig. 14b). As the pluton grew, and became large, accumulated magmatic heat overwhelmed emplacement-related cooling effects and deformation was dominantly in crystal mushes under PFC conditions (Fig. 14d). This is evident towards the pluton core. Deformation of thermally-softened wall-rock by an expanding pluton during later-stage magma addition may have resulted in more equant shapes (Rubin, 1995b; Fowler, 1994). This seems to be the case for the Creswick Gap pluton (Vaughan and Millar, 1996). The smaller Burns Bluff pluton appears to have remained largely tabular. Sheet-like emplacement modified by extensional shear produced a compositionally layered Burns Bluff pluton. This is a frequently overlooked, but widely developed feature of granite *s.l.* plutons (e.g. Duke et al., 1988; Gasquet et al., 1995).

6.4. Fault system geometry and timing

During continued extension in the cooling Creswick Gap pluton at Creswick Peaks, distributed PFC shear was replaced by ductile shear in decametre-scale zones focused at the pluton margin (Vaughan and Millar, 1996). This late, pluton-marginal ductile shear zone hosted syn-extensionally deformed gabbro (Fig 14a; Vaughan and Millar, 1996) as that at Moore Point (Fig. 3). At Burns Bluff, the shear zone partly hosted the Burns Bluff pluton (Fig. 14b). The relationship between the steeper Burns Bluff pluton and more shallowly-dipping Creswick Gap pluton shear zone (e.g. Fig. 4c) suggest that the Burns Bluff pluton may have been emplaced in a shear zone forming a second generation normal “fault” to the Creswick Gap pluton shear zone. This is more commonly seen in sedimentary basins

(Jackson and White, 1989), but is a likely outcome in evolving systems of extensional structures because shear zones rotate towards horizontal as they develop. Second generation structures start to form once the previous generation have rotated to a dip of 30° (Jackson and White, 1989). An implication of fault-system-like control on pluton emplacement is that the Wiley Glacier complex was emplaced above the base of the brittle–ductile transition (approximately 15–18 km depth, Jackson and McKenzie, 1983).

U–Pb and Ar–Ar ages combine to suggest that magmatic activity was concentrated between 145 and 140 Ma, whereas extensional shearing continued until 127 Ma. This is long compared to the duration of extensional shear zones in metamorphic core complexes (Hacker et al., 1990), and suggests either low rates of exhumation, or episodic shear zone activity at higher exhumation rates.

6.5. Geophysical evidence for underplating and intraplating

The most obvious expressions of crustal growth in the Wiley Glacier complex are the large gabbro body at Moore Point, and hornblende gabbro and quartz diorite at Burns Bluff. These have isotopic and chemical compositions that are consistent with a predominantly mantle origin. Although the gabbro–diorite intrusions crop out over a small area (Fig. 3), exposures of Cretaceous gabbro in western Palmer Land coincide with extensive magnetic (Renner et al., 1985; Maslanyj et al., 1991; Johnson and Smith, 1992) and residual gravity anomalies (Garrett, 1990). The extent of these geophysical anomalies suggests that large volumes of mafic mid-crustal rocks are present beneath the ice or at shallow crustal levels. These mafic rocks were probably intraplated and underplated as magma at mid- to deep crustal levels during the Cretaceous and subsequently uplifted. *In situ*, underplated mafic

magma is suggested by a *ca* 15 km thick section of flat lying or shallowly dipping, high velocity (V_p *ca* 7.1 kms^{-1}), lower crustal seismic reflectors above the Moho in the northern Antarctic Peninsula (Conway, 1992), although the age of these is unknown.

6.6. Mantle signatures and sources

The close temporal and spatial association between gabbro and diorite in the Wiley Glacier complex and extensional shearing suggests strongly that structural discontinuities assist the emplacement of mantle-derived magmas into the crust (Vaughan and Millar, 1996; this study). Although tonalite–granodiorite units within the Burns Bluff pluton assimilated continental crust, they have anomalously high ϵNd values compared to contemporaneous plutonism elsewhere in western Palmer Land. This suggests that they may have a correspondingly larger mantle component (cf. Fig. 13). Because extensional shear zones can focus the emplacement of mantle magma into the crust, we would expect shear-zone-hosted granitoids to have a larger mantle component, and thus have higher ϵNd than those elsewhere. The high ϵNd of the Burns Bluff pluton (Fig. 13) is strong evidence in favour of this.

6.7. Crustal structure and the granite “room” problem

The large volumes of mafic magma emplaced in northwestern Palmer Land during the Early Cretaceous suggest bulk pure shear extension of the lithosphere (Latin and White, 1990), although pluton-hosting shear zones predominantly dip east, apart from the west-dipping shear zone hosting granodiorite at Mount Eissenger (Fig. 2) (Vaughan and Millar, 1996). A reconstructed section through the Early Cretaceous crust of western Palmer Land

(Fig. 15) shows coeval east- and west-dipping shear zones, with the Mount Eissenger shear zone antithetic to the cross-cutting Burns Bluff and Creswick Gap pluton shear zones. Projection of the Burns Bluff pluton shear zone to the base of the crust in Fig. 15 is purely conjectural, although such structures are frequently imaged on deep seismic sections (e.g. Cosca et al., 1995). As discussed above, these structures would provide an easy path to mid-crustal levels for granitoid magma generated from mantle magma by fractionation or remelting of mafic underplate. Overall, dyke-like emplacement in extensional shear zones for the Wiley Glacier complex and Mount Eissenger plutons suggests that the continental crust was “spreading”, although by a more complex mechanism than that for the emplacement of vertical dykes observed at mid-ocean ridges. It is not possible to say given the data from the Wiley Glacier complex if spreading was symmetric or asymmetric.

In the context of the granite “room” problem (Paterson and Fowler, 1993), “continental spreading” is a good way of making space locally for granites in the crust, i.e. near field extension. However, on a larger scale, far-field extension transfer of material in the crust or mantle is also required to compensate for the space taken up by an intruding pluton (Paterson and Fowler, 1993). Although gravitational spreading of an overthickened arc pile could provide a mechanism for far-field extension, a simpler mechanism is likely to be pull of the subducting slab and rolling back of the hinge. Both of these processes are driven by sinking of oceanic lithosphere into the mantle, an excellent candidate for the compensatory material transfer process required by Paterson and Fowler (1993). The widespread evidence for extension in arcs (Hamilton, 1994) suggests that far-field, tensional, subduction forces produced near-field extension on shear zones in the Antarctic Peninsula magmatic arc and thus room for the plutons of the Wiley Glacier complex. Similar crustal growth complexes are seen in Early Cretaceous granitoids in north Chile (Dallmeyer et al., 1996), Patagonia

Vaughan, Wareham and Millar
(Grocott et al., 1994) and New Zealand (Tulloch and Kimbrough, 1989).

7. Conclusions

1) Isotopic data suggest that:

A) The plutons of the Wiley Glacier complex are fractionated, mantle-derived magmas, with different proportions of assimilated Palmer Land basement gneiss.

B) Shear-zone-hosted granites *s.l.* of the Wiley Glacier complex have higher ϵ_{Nd} than contemporaneous plutonism elsewhere in western Palmer Land and correspondingly have a larger mantle component.

2) Radiometric dating and the relationship between the Creswick Gap pluton and the slightly younger Burns Bluff pluton suggests that:

A) the plutons and their associated shear zones form “primary” and “secondary” structures in a system of extensional shears, and

B) that the Burns Bluff pluton was probably emplaced close to the brittle–ductile transition at a depth of 15–18 km.

C) that although magmatism appears to be concentrated at *ca* 141 Ma, extensional shearing may have been active from 145–127 Ma.

3) Isotopic data, and the current exposure of mid-crustal, coeval granitic *s.l.* and gabbroic rocks west of Creswick Gap in northwest Palmer Land suggest that "continental spreading" drove crustal growth by:

A) providing conduits for additions of mantle-derived magma at deep crustal levels (> 50 km depth). This magma underplated and intraplated the lower crust.

B) redistributing the granitic *s.l.* and mafic products of fractionated, remelted, or crustally contaminated mantle-derived magmas to mid-crustal levels during arc extension with shear zone-hosted dyking and pluton formation.

4) The wide geographical distribution of Early Cretaceous extensional magmatic complexes suggests a large province of crustal growth and consolidation along the Pacific margin of Gondwana.

Acknowledgements

The authors would like to thank the field and air operations staff at Rothera Base for logistical support. The assistance of Paul Thompson in the field is gratefully acknowledged. We would also like to thank Pete Bucktrout who printed the photographic figures and Bryan Storey who reviewed an early draft of the manuscript.

References

Atherton, M. P. and Petford, N., 1993. Generation of sodium-rich magmas from newly

Vaughan, Wareham and Millar
underplated basaltic crust. *Nature*, 362: 144–146.

Carrigan, C. R., Schubert G. and Eichelberger J. C., 1992. Thermal and dynamical regimes of single- and two-phase magmatic flow in dykes. *J. Geophys. Res.*, 97: 17377–17392.

Conway, A. M., 1992. Crustal Structure off the Antarctic Peninsula South West of Anvers Island. Ph.D. thesis. Birmingham University, England 189 pp.

Corfu, F. and Ayres, L. D., 1984. U–Pb ages and genetic significance of heterogeneous zircon populations in rocks from the Favourable Lake area, northwestern Ontario. *Contrib. Mineral. Petrol.*, 88: 86–101.

Cosca, M. A., Essene, E. J., Meszger, K. and van der Pluijm, B. A., 1995. Constraints on the duration of tectonic processes: protracted extension and deep-crustal rotation in the Grenville orogen. *Geology*, 23: 361–364.

Dallmeyer, R. D., Brown, M., Grocott, J., Taylor, G. K. and Treloar, P. J., 1996. Mesozoic magmatic and tectonic events within the Andean plate boundary zone, 26°–27°30'S, north Chile: constraints from $^{40}\text{Ar}/^{39}\text{Ar}$ ages. *J. Geol.*, 104: 19–40.

DePaolo, D. J., 1981. Neodymium isotopes in the Colorado Front Range and crust-mantle evolution in the Proterozoic. *Nature*, 291: 193–196.

DePaolo, D. J., Linn, A. M. and Schubert, G., 1991. The continental crustal age distribution: methods of determining mantle separation ages from Sm–Nd isotope data and

Vaughan, Wareham and Millar
applications to the southwestern United States. *J. Geophys. Res.*, 96: 2071–2088.

Duke, E. F., Redden, J. A. and Papike, J. J., 1988. Calamity Peak layered granite–pegmatite complex, Black Hills, South Dakota: part 1. structure and emplacement. *Bull. Geol. Soc. Am.*, 100: 825–840.

Fitches, W. R., Cave, R., Craig, J. and Maltman, A. J. C., 1986. Early veins as evidence of detachment in the Lower Paleozoic rocks of the Welsh Basin: *J. Struct. Geol.*, 8: 607–620.

Fowler, T. J., 1994. Sheeted and bulbous pluton intrusion mechanisms of a small granitoid from southeastern Australia: implications for dyke-to-pluton transformation during emplacement. *Tectonophysics*, 234: 197–215.

Gasquet, D., Fernandez, A., Mahé, C. and Boullier, A. M., 1995. Origine des rubanements dans les granitoïdes: exemple du monzogranite de Brignogan–Plouescat (NW du Massif armoricain). *C. R. Acad. Sci. Paris*, 321: 369–376.

Garrett, S. W., 1990. Interpretation of reconnaissance gravity and aeromagnetic surveys of the Antarctic Peninsula. *J. Geophys. Res.*, 95: 6759–6777.

Grocott, J., Brown, M., Dallmeyer, R. D., Taylor, G. K. and Treloar, P. J., 1994. Mechanisms of continental growth in extensional arcs: An example from the Andean plate-boundary zone. *Geology*, 22: 391–394.

- Hacker, B. R., Yin, A., Christie, J. M. and Snoke, A. W., 1990. Differential stress, strain rate, and temperature of mylonitization in the Ruby Mountains, Nevada: implications for the rates and duration of uplift. *J. Geophys Res*, 95: 8569–8580,
- Hamilton, W. B. 1994. Subduction systems and magmatism. In: J. L. Smellie (Editor), *Volcanism Associated with Extension at Consuming Plate Margins*. Geol. Soc. Spec. Pub., 81: 3–28.
- Hancock, P. L., 1972. The analysis of en echelon veins. *Geol. Mag.*, 109: 269–276.
- Hanson, R. B. and Glazner, A. F., 1995. Thermal requirements for extensional emplacement of granitoids: *Geology*, 23: 213–216.
- Harrison, S. M., 1989. Aspects of magmatism and metamorphism within a magmatic arc: Evidence from north-western Palmer Land, Antarctic Peninsula. Ph.D. thesis. Council for National Academic Awards, England. 197 pp.
- Hawkesworth, C. J. and Norry, M. J., 1983. *Continental basalts and mantle xenoliths*. Shiva, Cheshire, 272 pp.
- Hole, M. J., 1986. Time-controlled geochemistry of igneous rocks of the Antarctic Peninsula. Ph.D. thesis. University of London, England. 396 pp.
- Hutton, D. H. W., 1988. Granite emplacement mechanisms and tectonic controls: inferences from deformation studies. *Trans. R. Soc. Edinb.*, 79: 245–255.

- Hutton, D. H. W., 1992. Granite sheeted complexes: evidence for the dyking ascent mechanism. *Trans. R. Soc. Edinb.*, 83: 377–382.
- Hutton, D. H. W., Dempster, T. J., Brown, P. E. and Becker, S. D., 1990. A new mechanism of granite emplacement: intrusion in active extensional shear zones. *Nature*, 343: 452–455.
- Jackson, J. A. and McKenzie, D. P., 1983. The geometrical evolution of normal fault systems. *J. Struct. Geol.*, 5: 471–482.
- Jackson, J. A. and White, N. J., 1989. Normal faulting in the upper continental crust: observations from regions of active extension. *J. Struct. Geol.*, 11: 15–36.
- Jacobsen, S. B. and Wasserburg, G. J., 1980. Sm-Nd isotope evolution of chondrites. *Earth Planet. Sci. Lett.*, 50: 149–155.
- Johnson, A. C. and Smith, A. M., 1992. New aeromagnetic map of West Antarctica (Weddell Sea sector): introduction to important features. In: Y. Yoshida, K. Kaminuma and K. Shiraishi (Editors), *Recent Progress in Antarctic Science*. Terrapub, Tokyo, pp. 555–562.
- Kelley, S. P., 1995. Ar–Ar dating by laser microprobe. In: P. J. Potts, J. F. W. Bowles, S. J. B. Reed and M. R. Cave (Editors), *Microprobe Techniques in the Earth Sciences*, Chapman and Hall, New York,

- Krogh, T. E., 1973. A low contamination method for the hydrothermal decomposition of zircon and extraction of U and Pb for isotopic age determinations. *Geochim. Cosmochim. Acta*, 37: 485–494.
- Krogh, T. E., 1982. Improved accuracy of U–Pb zircon ages by the creation of more concordant systems using an air abrasion technique. *Geochim. Cosmochim. Acta*, 46: 637–649.
- Krogh, T. E. and Davis, G. L., 1985. The production and preparation of ^{205}Pb for use as a tracer for isotope dilution analysis. *Carnegie Institute of Washington, Yearbook*, 74: 416–417.
- Latin, D. and White, N., 1990. Generating melt during lithospheric extension: pure shear vs. simple shear. *Geology*, 18: 327–331.
- Ludwig, K. R., 1989. PBDAT: a computer program for processing Pb–U–Th isotope data, version 1.20. US Geol. Surv., Open-file report 88-542.
- Ludwig, K. R., 1990. Isoplot: a plotting and regression program for radiogenic isotope data, version 2.03. US Geol. Surv., Open-file report 88-557.
- Maslanyj, M. P., Garrett, S. W., Johnson, A. C., Renner, R. G. B. and Smith, A. M., 1990. Aeromagnetic anomaly map of West Antarctica (Weddell Sea sector). BAS GEOMAP Series, Sheet 2, 1:2,500,000, with supplementary text. British Antarctic Survey,

Cambridge.

Milne, A. L. and Millar, I. L., 1989. The significance of mid-Palaeozoic basement in Graham Land, Antarctic Peninsula. *J. Geol. Soc. London*, 146: 207–210.

Pankhurst, R. J. and Rapela, C. R., 1995. Production of Jurassic rhyolite by anatexis of the lower crust of Patagonia. *Earth Planet. Sci. Lett.*, 134: 23–36.

Passchier, C. W. and Simpson, C., 1986. Porphyroclast systems as kinematic indicators, *J. Struct. Geol.*, 8: 831–843,

Paterson, S. R. and Fowler, T. K., 1993. Re-examining pluton emplacement processes. *J. Struct. Geol.*, 15: 191–206.

Paterson, S. R., Vernon, R. H. and Tobisch, O. T., 1989. A review of criteria for the identification of magmatic and tectonic foliations in granitoids. *J. Struct. Geol.*, 11: 349–363.

Petford, N., Kerr, R. C., and Lister, J. R., 1993. Dike transport of granitoid magmas. *Geology*, 21: 845–848.

Piercy, B. A. and Harrison, S. M., 1991. Mesozoic metamorphism, deformation and plutonism in the southern Antarctic Peninsula: evidence from north-western Palmer Land. In: M. R. A., Thomson, J. A. Crame, and J. W. Thomson (Editors), *Geological Evolution of Antarctica*. Cambridge University Press, Cambridge, pp.381–386.

Pitcher, W. S., 1993. *The Nature and Origin of Granite*. Blackie Academic and Professional, Glasgow, 321 pp.

Ramsay, J. G. and Huber, M., 1983. *The Techniques of Modern Structural Geology, Vol. 1: Strain Analysis*. Academic Press, London, 307 pp.

Renner, R. G. B., Sturgeon, L. J. S. and Garrett, S.W., 1985. Reconnaissance gravity and aeromagnetic surveys of the Antarctic Peninsula. *Brit. Ant. Surv. Sci. Rep.*, No. 110, 55 pp.

Rex, D. C. and Guise, G. G., 1995. Evaluation of argon standards with special emphasis on time scale measurements. In: G. S. Odin (editor), *Phanerozoic Time Scale*, Bull. Liais. Inform. IUGS Subcom. Geochronol., 13, Offset, Paris, 21–23.

Rooney, T. P., Riecker, R. E. and Gavasci, A. T., 1975. Hornblende deformation features. *Geology*, 3: 364–366.

Rothery, E., 1988. En echelon vein array development in extension and shear. *J. Struct. Geol.*, 10: 63–71.

Rubin, A. M., 1995a. Getting granite dikes out of the source region. *J. Geophys. Res.*, 100: 5911–5929.

Rubin, A.M., 1995b. On the thermal viability of dykes leaving magma chambers. *Geophys.*

- Samson, S. D. and Alexander, E. C., 1995. Calibration of the interlaboratory $^{40}\text{Ar}/^{39}\text{Ar}$ dating standard, MMHb-1. *Chem. Geol.*, 66: 27–34.
- Stacey, J. S. and Kramers, J. D., 1975. Approximation of terrestrial lead isotope evolution by a two-stage model. *Earth Planet. Sci. Lett.*, 26: 207–221.
- Steiger, R. H. and Jäger, E., 1977. Subcommittee on geochronology: convention on the use of decay constants in geo- and cosmochronology. *Earth Planet. Sci. Lett.*, 36: 359–362.
- Storey, B. C., Vaughan A. P. M. and Millar I. L., 1996. Geodynamic evolution of the Antarctic Peninsula during Mesozoic times and its bearing on Weddell Sea history. In: B. C. Storey, E. C. King and R. L. Livermore (Editors), *Weddell Sea tectonics and Gondwana breakup*. *Spec. Pub. J. Geol. Soc. London*, 108: 87–104.
- Tulloch, A. J. and Kimbrough, D. L., 1989. The Paparoa metamorphic core complex, New Zealand: Cretaceous extension associated with fragmentation of the Pacific margin of Gondwana. *Tectonics*, 8: 1217–1234.
- Vaughan, A. P. M. and Millar, I. L., 1996. Early Cretaceous magmatism during extensional deformation within the Antarctic Peninsula magmatic arc. *J. S. Am. Earth Sci.*, 9: 121–129.

Vaughan, Wareham and Millar

Vaughan, A. P. M., Thistlewood, L. and Millar, I. L., 1995. Brevia -Short notes: Small-scale convection at the interface between stratified layers of mafic and silicic magma, Campbell ridges, Palmer Land, Antarctica: syn-magmatic way-up criteria. *J. Struct. Geol.*, 17: 1071–1075.

Wareham, C. D. and Millar, I. L., 1995. Crustal evolution and the generation of magmas akin to adakites in western Palmer Land, Antarctic Peninsula. *US Geol. Surv. Circ.*, No. 1129: 157–158 (abstr.).

Wever, H. E., Millar I. L. and Pankhurst, R. J., 1994. Geochronology and radiogenic isotope geology of Mesozoic rocks from eastern Palmer Land, Antarctic Peninsula: crustal anatexis in arc-related granitoid genesis. *J. S. Am. Earth Sci.*, 7: 69–83

Appendix 1

U–Pb method dating analytical techniques

Zircons for U–Pb analysis were separated from samples using standard crushing and heavy mineral separation techniques. Zircon fractions were hand-picked under methanol, and only clear grains with no visible cracks or cores were analysed. All fractions were abraded (Krogh, 1982), then washed in 4N HNO₃ and H₂O to remove all traces of pyrite. U and Pb were extracted using standard methods (Krogh, 1973; Corfu and Ayres, 1984). Fractions were spiked with a mixed ²⁰⁵Pb+²³⁵U isotopic tracer prior to digestion and chemistry (Krogh and Davis, 1985). U and Pb were loaded together onto outgassed single Re filaments with silica gel and phosphoric acid. Isotope analyses were performed at the

Vaughan, Wareham and Millar

NERC Isotope Geosciences Laboratory, Keyworth, on a VG 354 mass-spectrometer using an ion-counting Daly detector. Pb isotope ratios were corrected for initial common Pb in excess of the laboratory blank using the common Pb evolution model of Stacey and Kramers (1975). Laboratory Pb and U blanks during the analysis of samples R.5284.1 and R.5287.1 were 6.5 pg and 2 pg, respectively. During the analysis of samples R.6063.5 and R.6057.6, these blanks had fallen to 4 pg and 1 pg, respectively. Ages were calculated using the decay constants recommended by Steiger and Jäger (1977). Data reduction was carried out using 'PBDAT' (Ludwig, 1989). The data were plotted using 'Isoplot' (Ludwig, 1990).

Appendix 2

Ar–Ar laserprobe method dating analytical technique

Ar–Ar laserprobe method dating was carried out by S. P. Kelley at the Open University, Milton Keynes, UK. Samples were washed in methanol and de-ionised water before being packed in aluminium foil and irradiated at the Ford reactor, University of Michigan. Upon return, individual grains were loaded into small, 2 mm-diameter, 2 mm-deep holes in an aluminium plate which was loaded in turn into a laser port with a fused silica window. Individual mica grains were fused with a focused, multimode beam from a Nd-YAG laser running at the fundamental wavelength of 1064 nm, using techniques described in Kelley (1995). Gas samples were gathered for a minimum of 5 minutes and equilibrated into an MAP215-50 noble gas mass spectrometer with a Johnston multiplier. All argon peaks were scanned 10 times and peak heights extrapolated back to the inlet time to allow for argon build-up and memory effects. The mean blank plus mass spectrometer backgrounds during the analyses were 2.4, 0.02 and 0.3×10^{-12} cc STP for ^{40}Ar , ^{39}Ar and ^{36}Ar respectively. Data

in Table 4 were corrected for mass spectrometer discrimination and irradiation interference reactions. Ages calculated were based upon analyses of the Tinto biotite standard (Rex and Guise, 1995) international standard MMHb1 assuming an age of 520.4 Ma (Samson and Alexander, 1987).

Appendix 3

Isotope geochemistry analytical techniques

Sample powders for isotope analysis were prepared from 3–5 kg of fresh rock. Samples were reduced to *ca* 3 cm³ chips with a hardened-steel hydraulic splitter, then crushed using a hardened-steel fly-press. A *ca* 500 g aliquot of <1200 μm sample was powdered using an agate swing mill. Isotope analyses were carried out at the NERC Isotope Geosciences Laboratory. Sr and Nd isotope compositions, and Sr, Rb, Sm and Nd concentrations, were analysed using standard techniques (e.g., Pankhurst and Rapela, 1995). ⁸⁷Sr/⁸⁶Sr is normalised to ⁸⁶Sr/⁸⁸Sr = 0.1194. Repeated analyses of NBS987 during the course of this study gave ⁸⁷Sr/⁸⁶Sr = 0.710190. ¹⁴³Nd/¹⁴⁴Nd is normalised to ¹⁴⁶Nd/¹⁴⁴Nd = 0.7219. Repeated analysis of Johnson–Matthey Nd yielded ¹⁴³Nd/¹⁴⁴Nd = 0.511122, corresponding to 0.511858 for the La Jolla standard. Maximum procedural blanks throughout the course of this study were <300 pg for Nd and Sr. εNd values were calculated using standard values of CHUR (Hawkesworth and Norry, 1983) and ¹⁴⁷Sm/¹⁴⁴Nd of 0.1967 (Jacobsen and Wasserburg, 1980). Single stage (T_{DM}) and multi-stage (T_{DM'}) depleted mantle Nd model ages were calculated using the equations of DePaolo (1981) and DePaolo et al. (1991) respectively.

FIGURE CAPTIONS

Fig. 1 Early Cretaceous (*ca* 140 Ma) plate reconstruction showing the position and tectonic setting of the Antarctic Peninsula in relation to the main crustal blocks of Gondwana (after Storey et al., 1996). Subduction zone (black line with filled triangles) is parallel to on-shore outcrop of Mesozoic arc rocks.

Fig. 2 Distribution of shear zones hosting Early Cretaceous plutons in western Palmer Land, Antarctic Peninsula. Double lines indicate plutonic complexes more than 1 km wide across strike. Note westward dip of the Mount Eissenger complex and southerly dip of the Auriga Nunataks complex.

Fig. 3 Geology of the Wiley Glacier Complex.

Fig. 4 U–Pb zircon data for plutons of the Wiley Glacier complex (A) inset showing the relationship between Burns Bluff tonalite–granodiorite and Creswick Gap quartz diorite wall rock (B) inset showing the relationship between Creswick Peaks and Renner Peak components of the Creswick Gap pluton. See text for explanation.

Fig. 5 (A) Ar–Ar isochron of biotite analyses from Creswick Gap granodiorite (B) Ar–Ar isochron of hornblende analyses from Creswick Gap granodiorite (C) Ar–Ar isochron of amphibole analyses from extensional ultramylonite zones in Creswick Gap granodiorite at Creswick Peaks.

Fig. 6 (A) Cliff section in sheeted western margin of Burns Bluff pluton. Layers dip from

right to left. Section is 200 m high. (B) Asymmetric microdiorite enclaves in Burns Bluff tonalite–granodiorite. Asymmetric enclaves are most abundant to immediate left of ice axe. Ice axe is 70 cm long. (C) Synmagmatically mylonitized sheet of Burns Bluff aplite cutting synmagmatically foliated Creswick Gap quartz diorite host pluton. Note normal-sense dragging of quartz diorite fabric at contact with aplite. Cord is 5 mm wide.

Fig. 7 Logged section at western Burns Bluff.

Fig. 8 Photomicrographs of oriented sections cut parallel to mineral stretching lineation. Field of view is 8.0 x 5.7 mm and up is towards top in each case. (A) Ductilely deformed "hornblende fish" in quartz diorite. (B) Imbricated plagioclase phenocrysts in quartz diorite. (C) Imbricated plagioclase porphyroclasts "floating" in mylonitized, porphyritic tonalite–granodiorite. (D) Plagioclase σ_a -porphyroclast in mylonitized, porphyritic tonalite–granodiorite. (E) Imbricated plagioclase grains in hypidiomorphic, weakly deformed tonalite–granodiorite. (F) Fractured plagioclase showing black, cross-cutting vein of "frozen" melt.

Fig. 9 (A) Lower hemisphere, equal area projection of lineation, fold plunge and poles to foliation for Creswick Gap quartz diorite. (B) The same data contoured. (C) Lower hemisphere, equal area projection of lineation, fold plunge and poles to foliation for Burns Bluff tonalite–granodiorite. (D) The same data contoured.

Fig. 10 (A) Plan view of Burns Bluff tonalite–granodiorite with irregular dykes and enclaves of microdiorite showing differing degrees of deformation. (B) Line-drawing

highlighting the features of (A). Notebook is 16 cm long.

Fig. 11 *En échelon* microdiorite dykes from main body of Burns Bluff tonalite–granodiorite.

Dykes may represent a "third order" array (Hancock, 1972) developed during dextral shear partitioning in an overall regime of transtension. Ornaments as Fig. 5. See section 4.6 for explanation.

Fig. 12 Schematic plan view of Burns Bluff tonalite–granodiorite pluton modelled as a large echelon structure. Ornaments as Fig. 5.

Fig. 13 $^{87}\text{Sr}/^{86}\text{Sr}$ vs $^{143}\text{Nd}/^{144}\text{Nd}$ plot corrected to 141 Ma for plutonic rocks exposed at western Burns Bluff. Inset is ϵNd_t vs age plot contrasting Wiley Glacier complex plutonic rocks with Triassic orthogneiss in the area (stars) and magmatism elsewhere in western Palmer Land (comparative data from Wareham and Millar, 1995). See text for explanation.

Fig. 14 (A) A ductile shear zone developed on the margin of the Creswick Gap pluton (numbered '1') as it cooled, but (B) during continued extension, a second pluton, the Burns Bluff tonalite–granodiorite (numbered '3') intruded the shear zone steeply oblique to the Creswick Gap pluton, initially as a series of sheets (C), but (D) did not grow large enough to reduce wall-rock viscosity and remained sheet-like. Moore Point gabbro is numbered '2'.

Fig. 15 Cartoon of a synoptic, Early Cretaceous, crustal section through western Palmer Land. Depths to boundaries across transition from brittle to ductile crust after Jackson

Vaughan, Wareham and Millar
and White (1989). Base of crust after Atherton and Petford (1993). Burns Bluff
tonalite–granodiorite (BB), Creswick Gap pluton (CG), Mount Eissenger granodiorite
(ME), Moore Point gabbro (MP); upper crust (UC), middle crust (MC), lower crust
(LC). See text.

Table 1. U–Pb zircon analyses for plutons of the Wiley Glacier complex

| | | Concentrations ² | | | | Atomic Ratios | | | | | | |
|---|---------------------|-----------------------------|---------|----------|----------------|---|---|--|--|---|---|----------------|
| Fraction ¹ | | Weight (μg) | U (ppm) | Pb (ppm) | Common Pb (pg) | ²⁰⁶ Pb/ ²⁰⁴ Pb ³ | ²⁰⁸ Pb/ ²⁰⁶ Pb ⁴ | ²⁰⁶ Pb/ ²³⁸ U ⁴ | ²⁰⁷ Pb/ ²³⁵ U ⁴ | ²⁰⁷ Pb/ ²⁰⁶ Pb ⁴ | ²⁰⁷ Pb/ ²⁰⁶ Pb Age (Ma) | ρ ⁵ |
| <i>Creswick Gap tonalite–granodiorite at Creswick Peaks, sample R.5287.1.⁶</i> | | | | | | | | | | | | |
| 1A | 30 grains, 150μ | 71.9 | 249.4 | 6.1 | 7.1 | 3635 | 0.1876 | 0.02268±7 | 0.1534±5 | 0.04907±8 | 151±3 | 0.90 |
| 1B | 56 grains, 80–110μ | 53.3 | 242.9 | 5.8 | 1.5 | 11804 | 0.2047 | 0.02219±9 | 0.1495±7 | 0.04887±10 | 141±5 | 0.89 |
| 1C | 6 grains, 225μ | 18.5 | 214.2 | 5.2 | 3.1 | 1811 | 0.1935 | 0.02218±2 4 | 0.1496±17 | 0.04892±17 | 144±6 | 0.97 |
| 1D | 50 grains, 80–120μ | 17.6 | 189.2 | 5.8 | 23.0 | 221 | 0.1966 | 0.02205±1 | 0.1489±12 | 0.04897±27 | 147±12 | 0.92 |
| <i>Creswick Gap granodiorite at Renner Peak, sample R.5284.1</i> | | | | | | | | | | | | |
| 1B | 10 grains, 200–300μ | 29.4 | 52.26 | 1.91 | 16.5 | 152 | 0.2794 | 0.02260±53 | 0.1538±41 | 0.04938±60 | 166±28 | 0.89 |
| 1 | 50 grains, 100μ | 39. | 88.10 | 2.36 | 0.3 | 17827 | 0.2664 | 0.02354±28 | 0.1602±20 | 0.04936±22 | 165±11 | 0.94 |
| <i>Creswick Gap diorite at Burns Bluff, sample R.6063.5</i> | | | | | | | | | | | | |
| 1A | 1 grain, 300 μ | 47.5 | 58.56 | 1.51 | 5.1 | 796 | 0.2005 | 0.02264±21 | 0.1540±16 | 0.04934±21 | 164±10 | 0.91 |
| 1C | 3 grains, 150–200 μ | 41.4 | 82.24 | 2.34 | 15.8 | 330 | 0.1791 | 0.02256±17 | 0.1528±15 | 0.04913±31 | 154±15 | 0.77 |
| 1 | 14 grains, 100 μ | 45. | 80.28 | 2.02 | 4.5 | 1192 | 0.1828 | 0.02257±16 | 0.1536±12 | 0.04937±15 | 165±7 | 0.92 |
| <i>Burns Bluff tonalite–granodiorite at Burns Bluff, sample R.6057.6</i> | | | | | | | | | | | | |
| 1C | 17 grains, 100 μ | 15.9 | 135.20 | 3.41 | 0.7 | 4243 | 0.2329 | 0.02257±2 7 | 0.1540±19 | 0.04950±20 | 172±10 | 0.95 |
| 1 | 25 grains, 80 μ | 10.3 | 136.91 | 6.0 | 28.9 | 84 | 0.2322 | 0.02127±3 | 0.1436±30 | 0.04898±70 | 147±34 | 0.74 |

- 1 Approximate number and grain-size of picked grains. All zircon grains were picked from the non-magnetic / non-diamagnetic split on a Frantz LB-1 Magnetic Barrier Separator. All grains were abraded prior to dissolution.
- 2 Errors on sample weights, and therefore on U and Pb concentrations, are approximately 20%.
- 3 Measured ratio corrected for fractionation and spike.
- 4 Corrected for fractionation, spike, laboratory Pb and U blanks, and initial common Pb (Stacey and Kramers, 1975). Measured laboratory Pb blank composition is: ²⁰⁶Pb/²⁰⁴Pb=17.549 ± 0.018; ²⁰⁷Pb/²⁰⁴Pb=15.548 ± 0.016; ²⁰⁸Pb/²⁰⁴Pb=37.323 ± 0.04. Assumed blanks for samples R.5287.1 and R.5284.1 are 6.5 pg for Pb and 2 pg for U. Assumed blanks for samples R.6063.5

and R.6057.6 are 4 pg for Pb and 1 pg for U. Errors on assumed blank concentrations are 50%. Errors are quoted at the 2s level, and refer to the last digits of isotopic ratios and ages. Data was reduced using the method of Ludwig (1980; 1989). Errors on measured ages propagated through the data reduction calculations were ± 2 standard errors of the mean.

5 Correlation coefficient of $^{207}\text{Pb}/^{235}\text{U}$ to $^{206}\text{Pb}/^{238}\text{U}$ is calculated using the procedures and algorithm of Ludwig (1980; 1989)

6 Creswick Peaks data from Vaughan and Millar (1996), recalculated using actual rather than assumed blank composition.

Table 2. Ar–Ar laserprobe mineral analyses for Creswick Gap tonalite–granodiorite

| Sample | $^{40}\text{Ar}/^{39}\text{Ar}$ | $^{38}\text{Ar}/^{39}\text{Ar}$ | $^{37}\text{Ar}/^{39}\text{Ar}$ | $^{36}\text{Ar}/^{39}\text{Ar}$ | $^{39}\text{Ar}^1$ | $^{40}\text{Ar}^*/^{39}\text{Ar}$ | \pm^2 | Age (Ma) | \pm^2 |
|----------------------|---------------------------------|---------------------------------|---------------------------------|---------------------------------|--------------------|-----------------------------------|---------|----------|---------|
| <i>Undeformed</i> | | | | | | | | | |
| R.5380.8 biotite 1 | 24.131 | 0.1160 | 0.3704 | 0.0102 | 34.23 | 21.13 | 0.88 | 169.1 | 6.8 |
| R.5380.8 biotite 2 | 20.755 | 0.0743 | 0.1237 | 0.0035 | 80.40 | 19.72 | 0.27 | 158.3 | 2.2 |
| R.5380.8 biotite 3 | 21.541 | 0.1104 | 0.3348 | 0.0084 | 17.36 | 19.06 | 0.42 | 153.2 | 3.3 |
| R.5380.8 biotite 4 | 20.771 | 0.1389 | 0.8489 | 0.0043 | 15.56 | 19.50 | 0.61 | 156.6 | 4.8 |
| R.5380.8 biotite 5 | 21.747 | 0.0721 | 0.2175 | 0.0083 | 7.41 | 19.31 | 0.79 | 155.1 | 6.1 |
| R.5380.8 biotite 6 | 22.147 | 0.0745 | 0.1617 | 0.0157 | 45.66 | 17.52 | 0.52 | 141.3 | 4.1 |
| R.5380.8 biotite 7 | 22.240 | 0.0944 | 0.3020 | 0.0132 | 33.03 | 18.34 | 0.52 | 147.6 | 4.1 |
| R.5380.8 biotite 8 | 19.781 | 0.1668 | 0.6396 | 0.0047 | 10.03 | 18.39 | 0.73 | 148.0 | 5.7 |
| R.5380.8 biotite 9 | 20.954 | 0.0798 | 0.4312 | 0.0105 | 29.86 | 17.84 | 0.42 | 143.8 | 3.3 |
| R.5380.8 biotite 10 | 21.675 | 0.1026 | 0.3413 | 0.0083 | 32.15 | 19.23 | 0.24 | 154.5 | 2.0 |
| <i>Undeformed</i> | | | | | | | | | |
| R.5380.8 Hb1 | 20.490 | 0.3415 | 1.9310 | 0.0121 | 17.20 | 16.90 | 0.83 | 136.5 | 6.5 |
| R.5380.8 Hb2 | 20.991 | 0.3722 | 1.9145 | 0.0023 | 38.06 | 20.30 | 0.25 | 162.7 | 2.1 |
| R.5380.8 Hb3 | 20.970 | 0.1352 | 0.7139 | 0.0045 | 75.77 | 19.65 | 0.13 | 157.7 | 1.3 |
| R.5380.8 Hb4 | 21.927 | 0.2593 | 2.1081 | 0.0070 | 18.60 | 19.86 | 0.40 | 159.4 | 3.2 |
| R.5380.8 Hb5 | 22.488 | 0.2713 | 1.8070 | 0.0054 | 36.46 | 20.88 | 0.32 | 167.2 | 2.6 |
| R.5380.8 Hb6 | 20.901 | 0.3532 | 2.3635 | 0.0049 | 17.87 | 19.46 | 0.41 | 156.3 | 3.3 |
| R.5380.8 Hb7 | 23.045 | 0.2223 | 1.3201 | 0.0096 | 64.52 | 20.20 | 0.21 | 162.0 | 1.8 |
| R.5380.8 Hb8 | 20.948 | 0.1119 | 0.4941 | 0.0041 | 32.04 | 19.74 | 0.32 | 158.5 | 2.6 |
| R.5380.8 Hb9 | 21.554 | 0.1884 | 1.0120 | 0.0039 | 69.13 | 20.40 | 0.20 | 163.5 | 1.7 |
| R.5380.8 Hb10 | 20.803 | 0.2947 | 1.8312 | 0.0018 | 46.07 | 20.26 | 0.22 | 162.4 | 1.8 |
| <i>Ultramylonite</i> | | | | | | | | | |
| R.5380.4a Amph 1 | 19.973 | 0.1604 | 3.1176 | 0.0017 | 14.83 | 19.46 | 0.27 | 142.6 | 2.0 |
| R.5380.4a Amph 2 | 29.532 | 0.2765 | 6.1818 | 0.0360 | 16.99 | 18.90 | 0.38 | 138.6 | 2.7 |
| R.5380.4a Amph 3 | 55.643 | 0.6396 | 4.8757 | 0.1150 | 5.74 | 21.67 | 1.11 | 158.0 | 7.8 |
| R.5380.4a Amph 4 | 37.446 | 0.3600 | 2.6382 | 0.0611 | 17.26 | 19.39 | 0.54 | 142.1 | 3.9 |
| R.5380.4a Amph 5 | 27.537 | 0.2594 | 4.7510 | 0.0327 | 19.19 | 17.88 | 0.35 | 131.4 | 2.5 |
| R.5380.4a Amph 6 | 72.979 | 0.5884 | 1.2151 | 0.1907 | 2.64 | 16.64 | 1.79 | 122.6 | 12.8 |
| R.5380.4a Amph 7 | 31.800 | 0.2977 | -3.9534 | 0.0503 | 6.39 | 16.94 | 1.02 | 124.7 | 7.3 |
| R.5380.4a Amph 8 | 32.688 | 0.3899 | -0.8609 | 0.0393 | 8.71 | 21.08 | 0.72 | 154.0 | 5.1 |
| R.5380.4a Amph 9 | 38.755 | 0.4773 | 4.2573 | 0.0658 | 8.28 | 19.30 | 0.76 | 141.4 | 5.4 |
| R.5380.4a Amph 10 | 46.952 | 0.8905 | 10.0291 | 0.0887 | 2.81 | 20.73 | 1.91 | 151.5 | 13.4 |
| R.5380.4a Amph 11 | 23.608 | 0.0977 | 0.7402 | 0.0204 | 28.37 | 17.58 | 0.31 | 129.3 | 2.3 |

| | | | | | | | | | |
|-------------------|--------|--------|--------|--------|-------|-------|------|-------|-----|
| R.5380.4a Amph 12 | 29.033 | 0.1441 | 1.1601 | 0.0396 | 18.10 | 17.33 | 0.40 | 127.5 | 2.9 |
|-------------------|--------|--------|--------|--------|-------|-------|------|-------|-----|

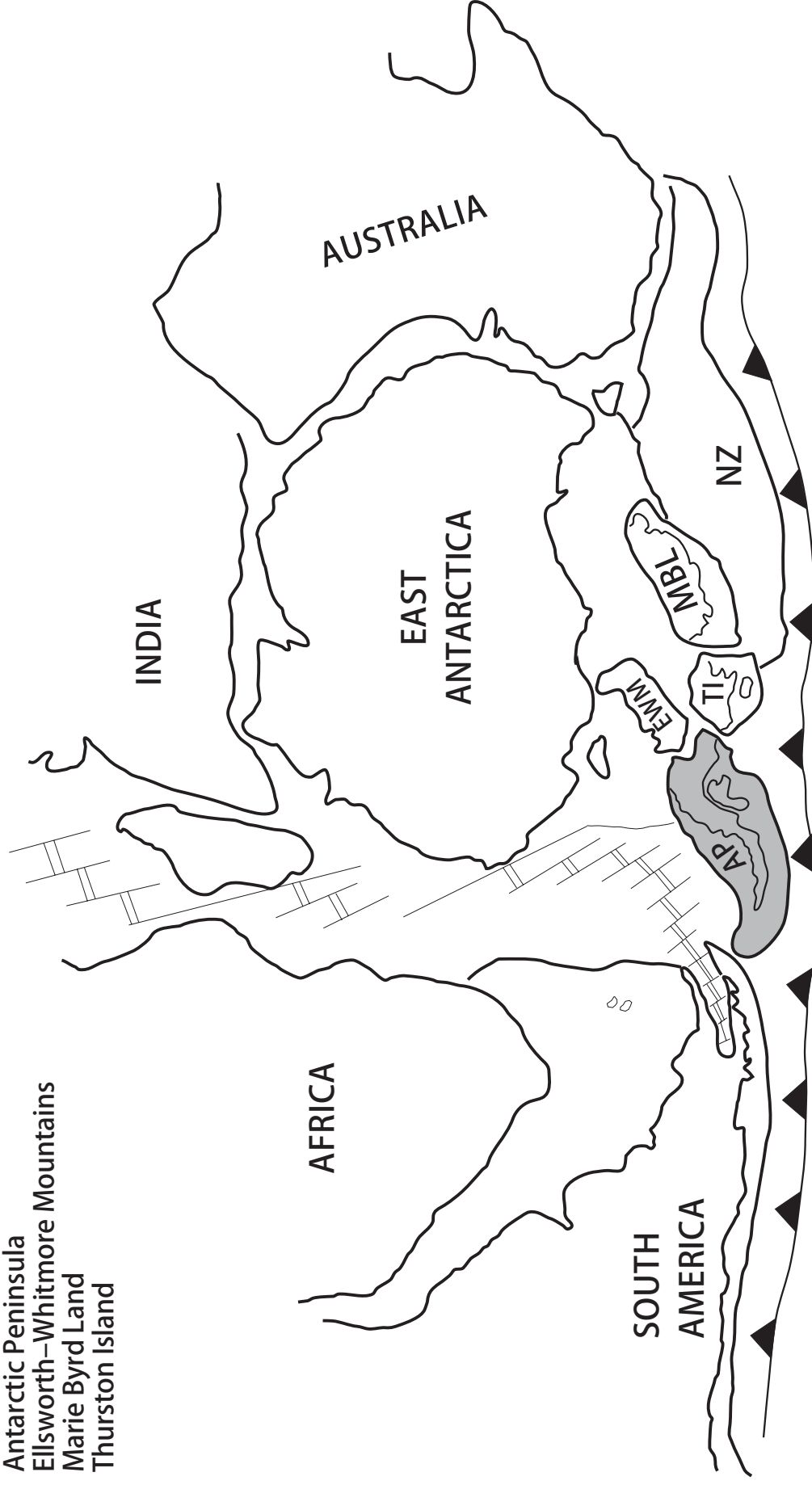
¹ ³⁹Ar amounts in 10⁻¹² cc STP

² Errors quoted at 1s level

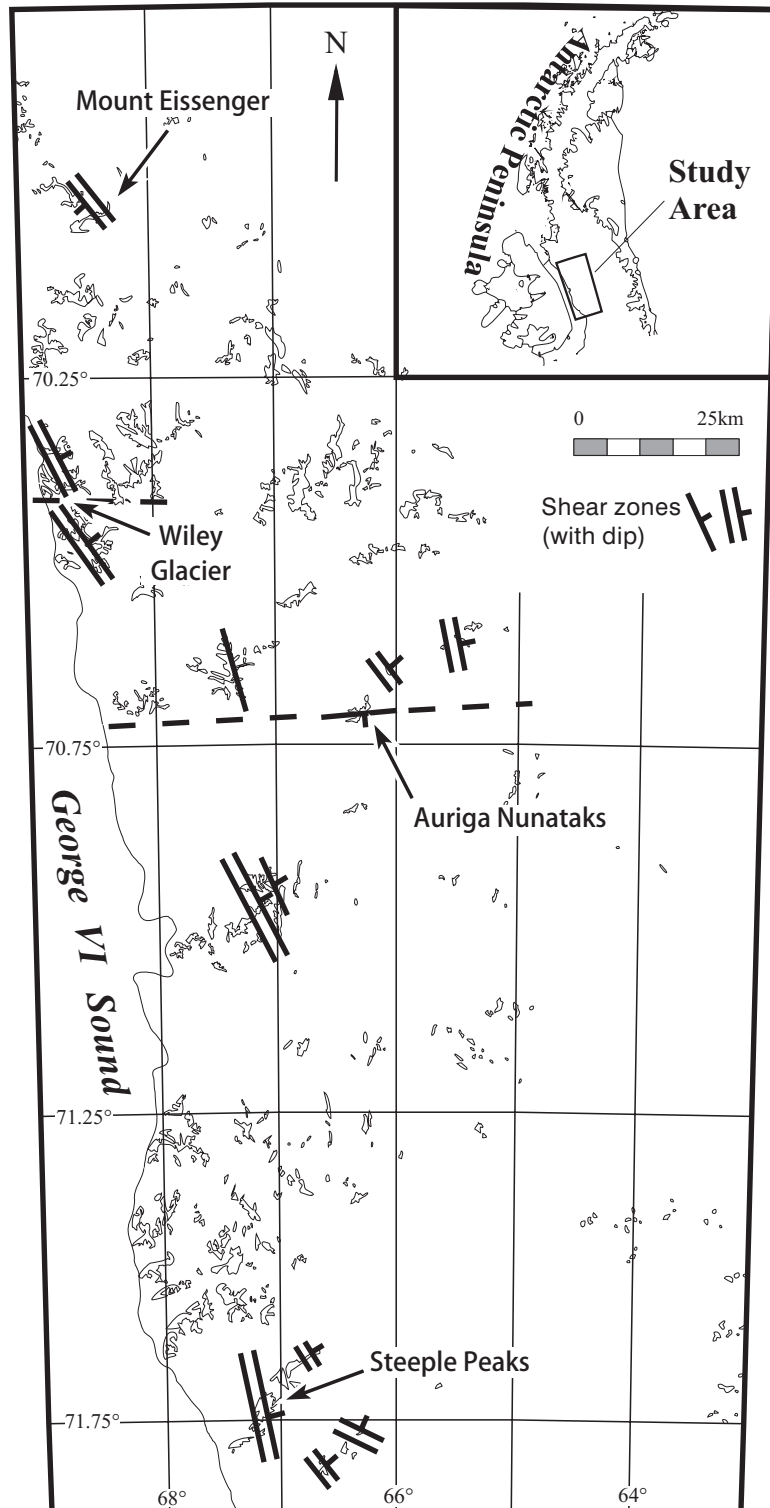
Early Cretaceous (ca 140 Ma)

Key

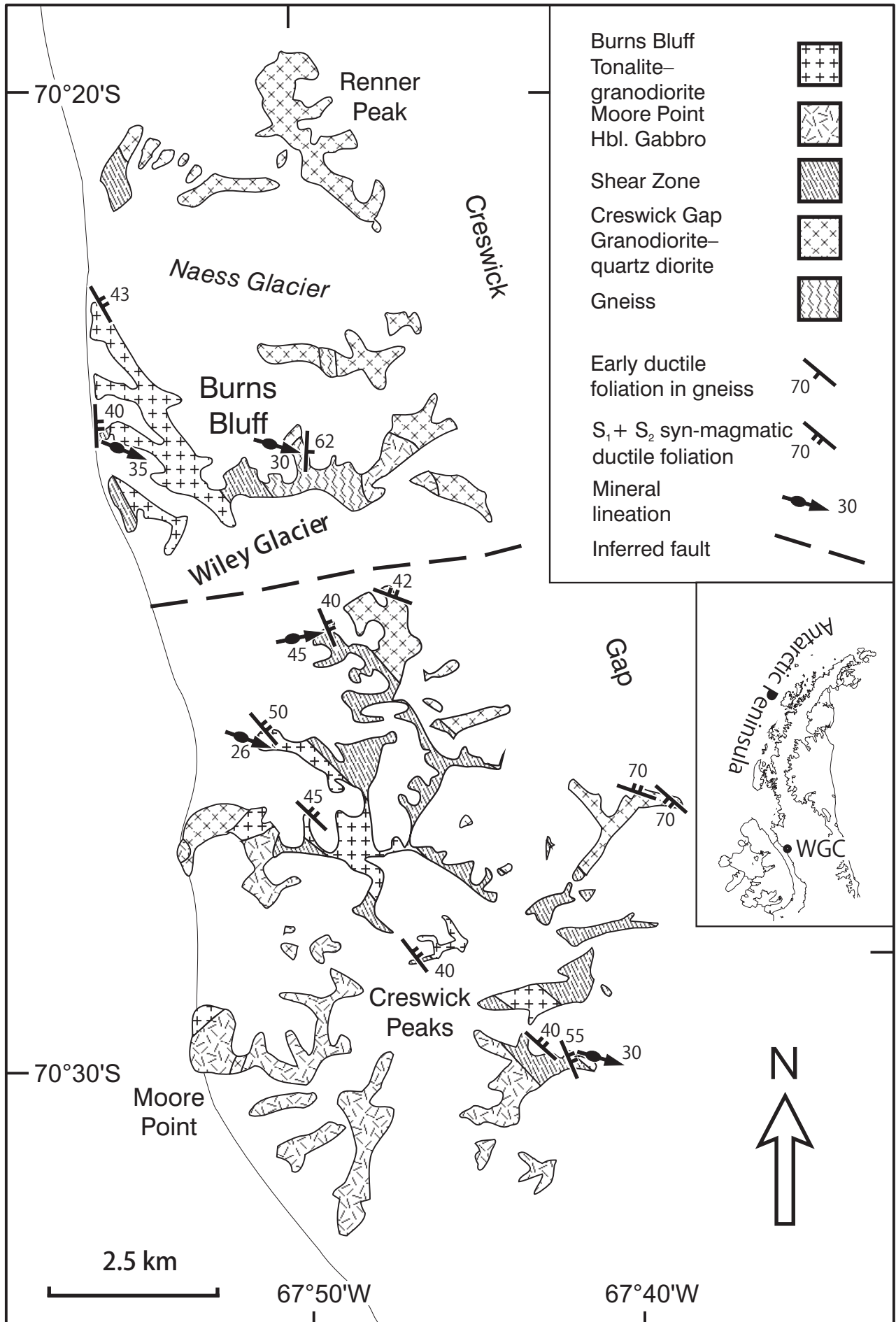
- AP Antarctic Peninsula
- EWM Ellsworth-Whitmore Mountains
- MBL Marie Byrd Land
- TI Thurston Island



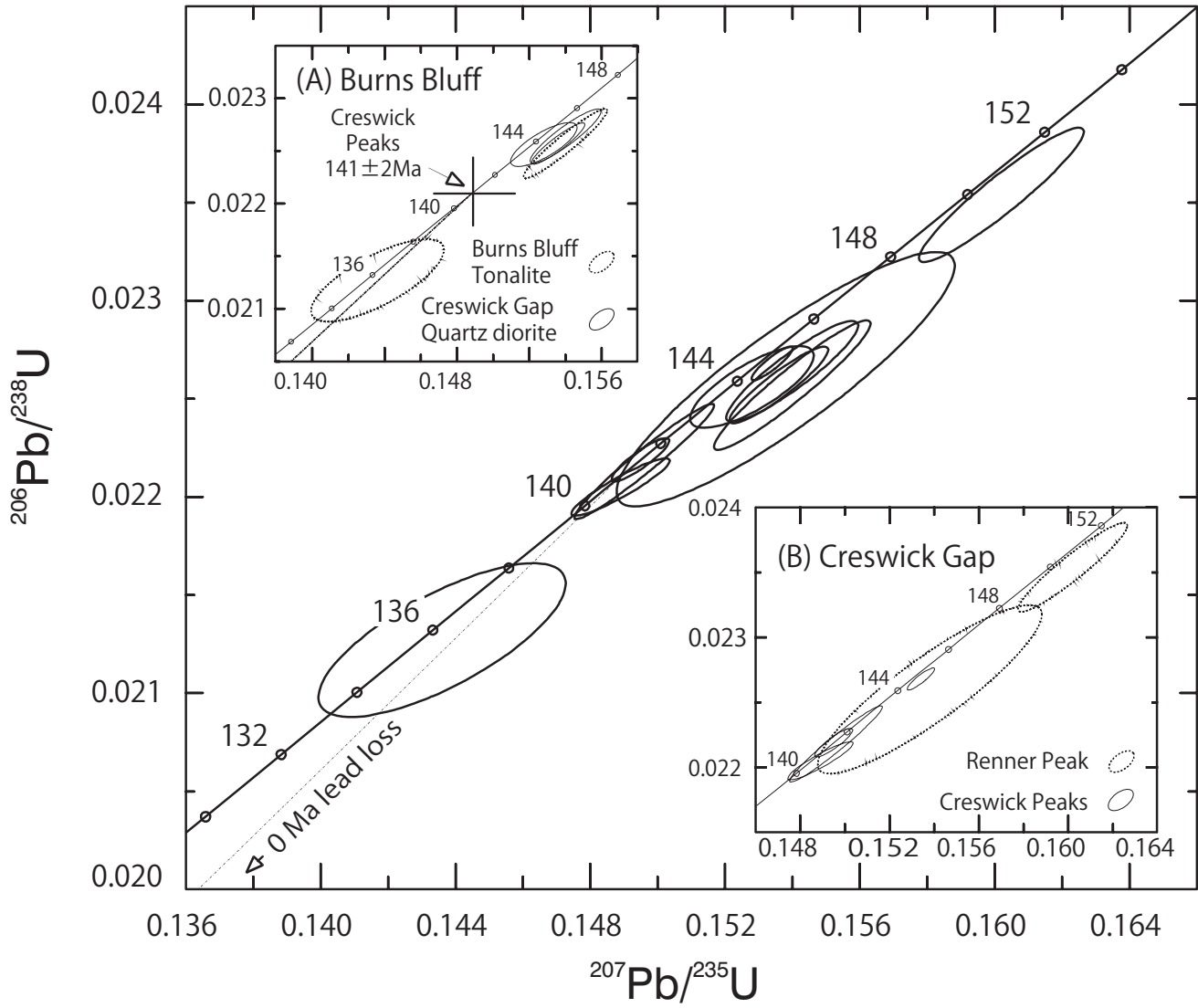
Vaughan, Wareham and Millar Fig. 2



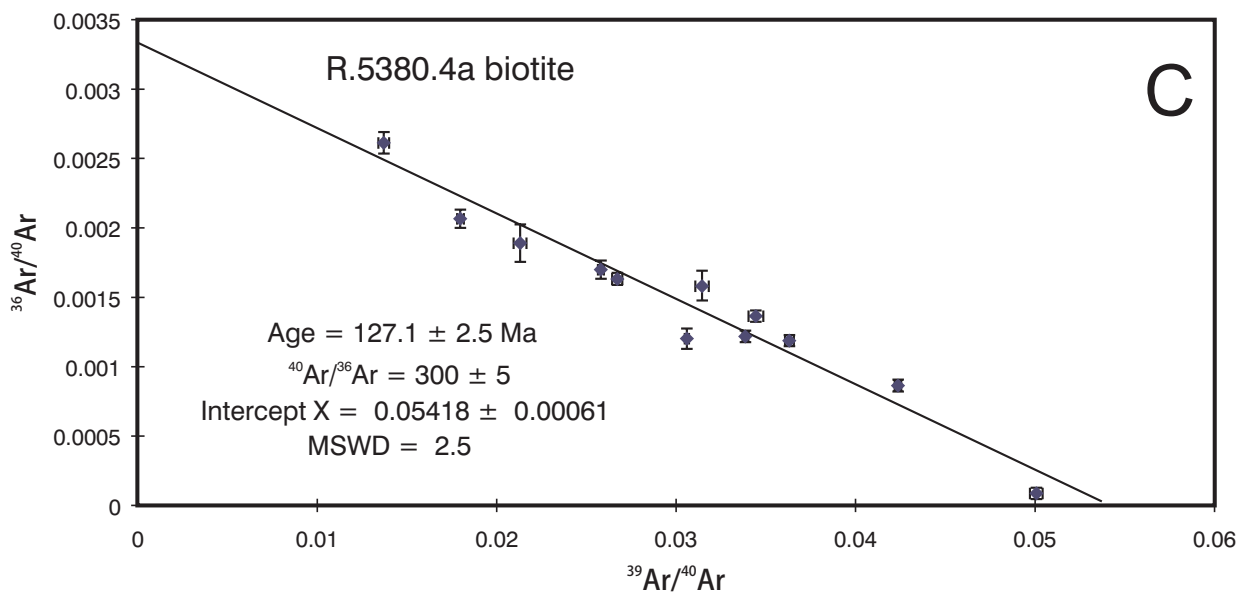
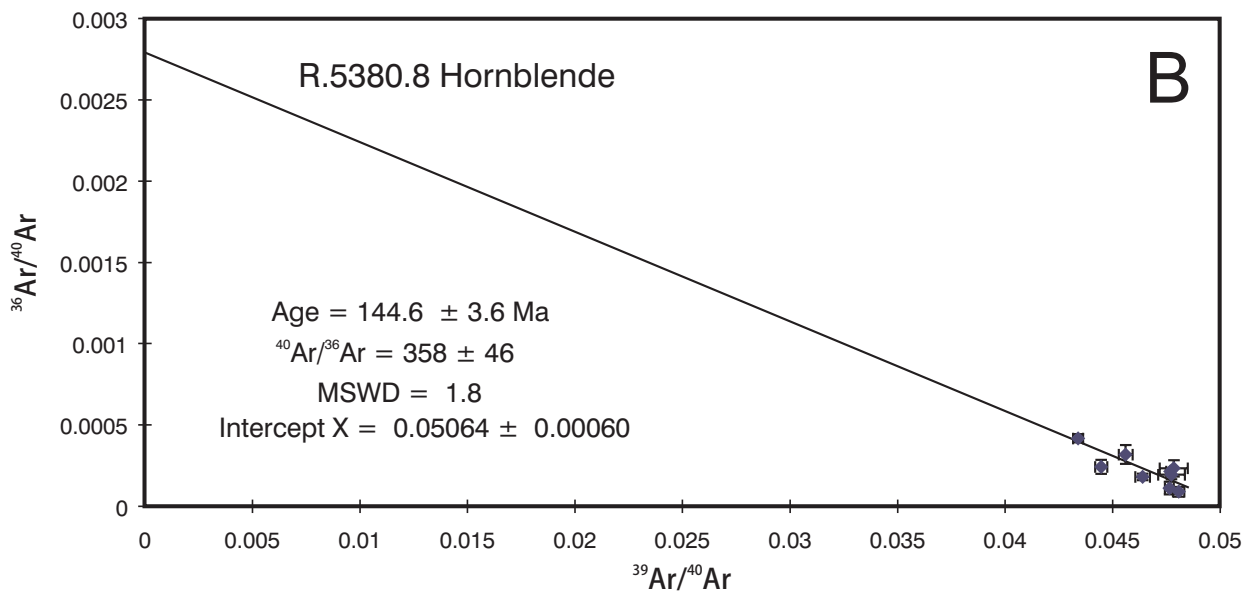
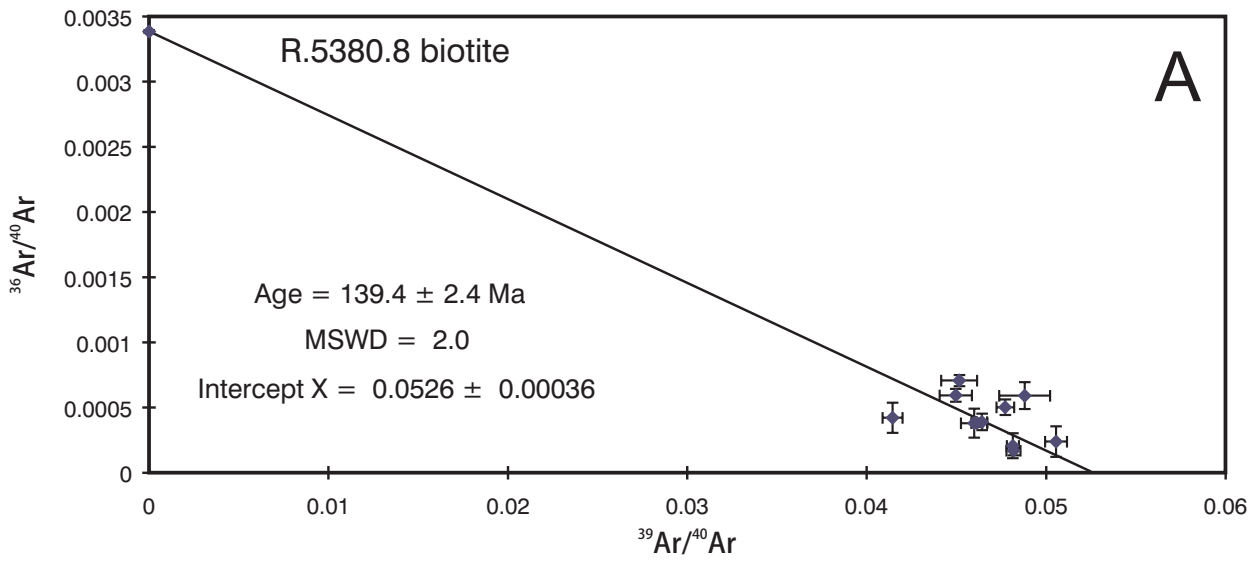
Vaughan, Wareham and Millar Fig. 3



Vaughan, Wareham and Millar Fig. 4



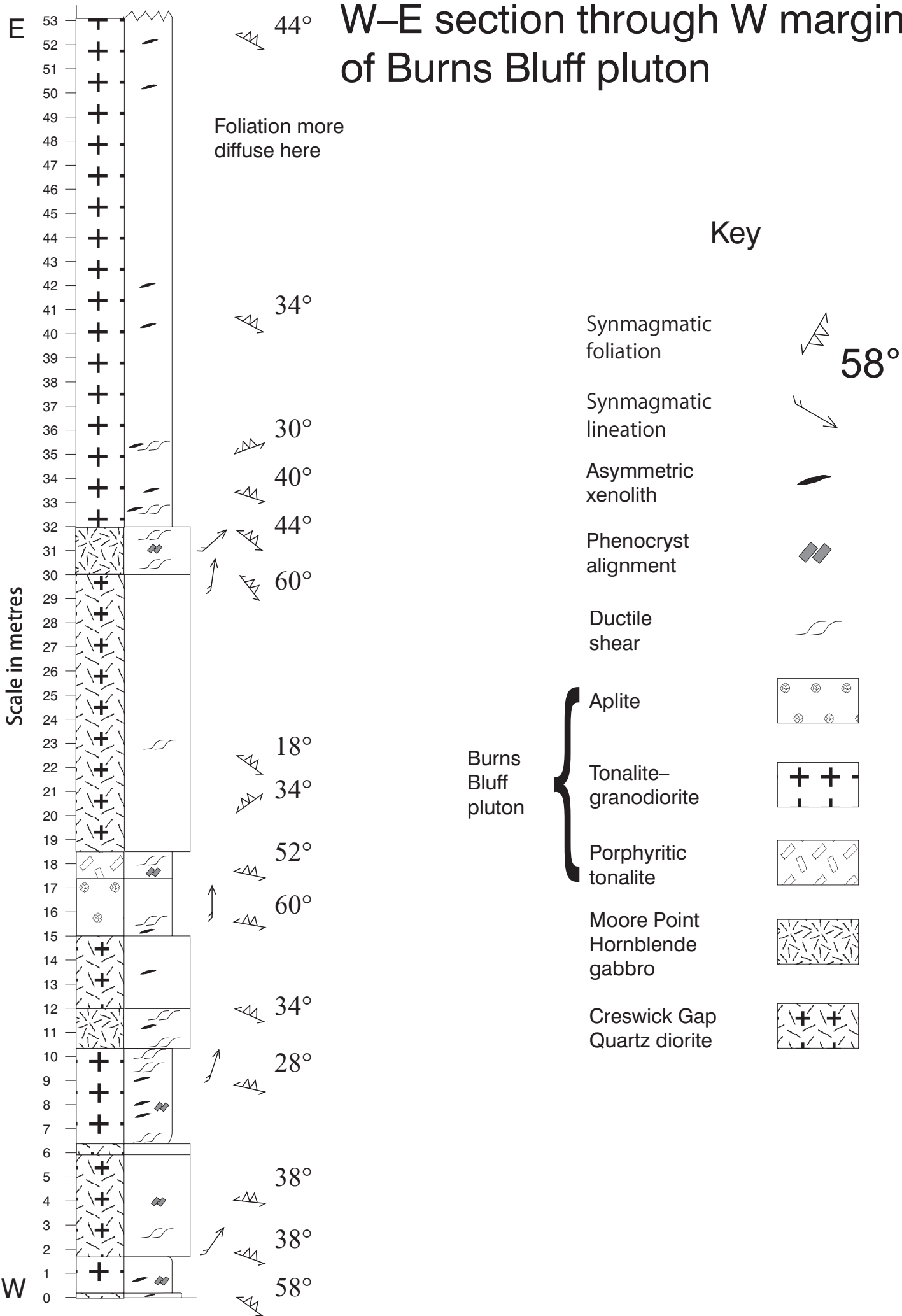
Vaughan, Wareham and Millar, Figure 5



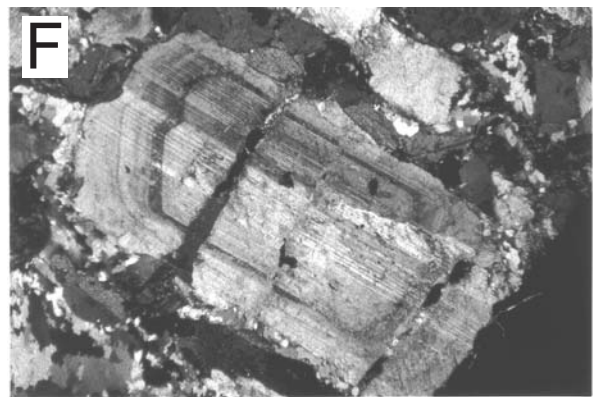
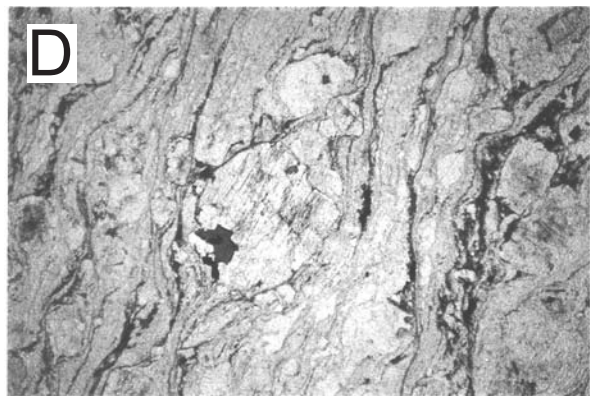
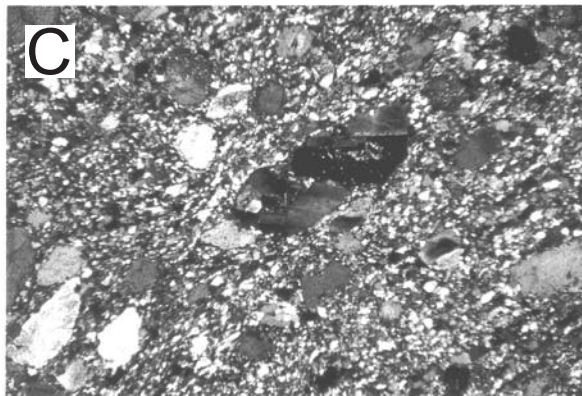
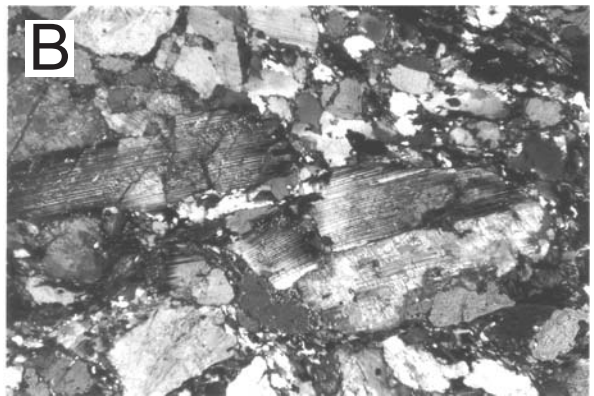
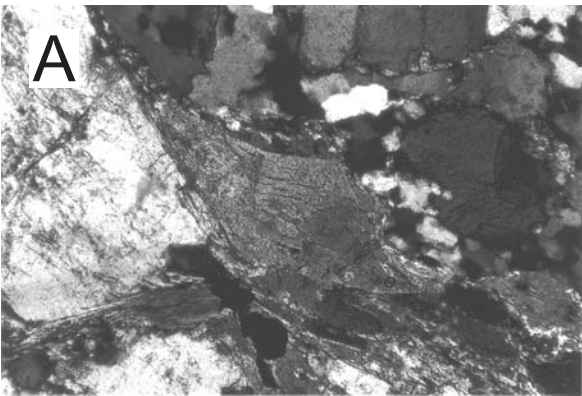
Vaughan, Wareham and Millar Figure 6



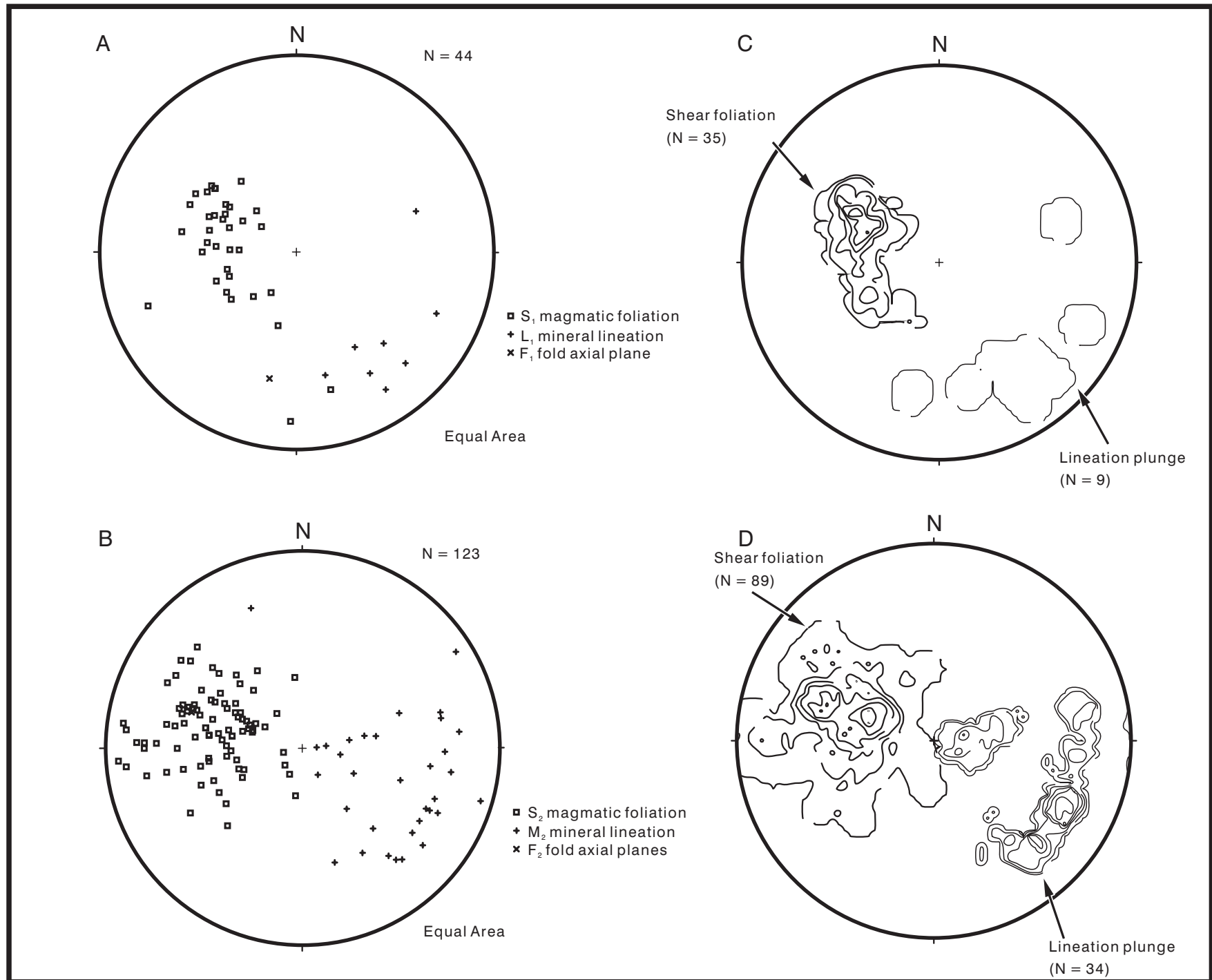
W-E section through W margin of Burns Bluff pluton



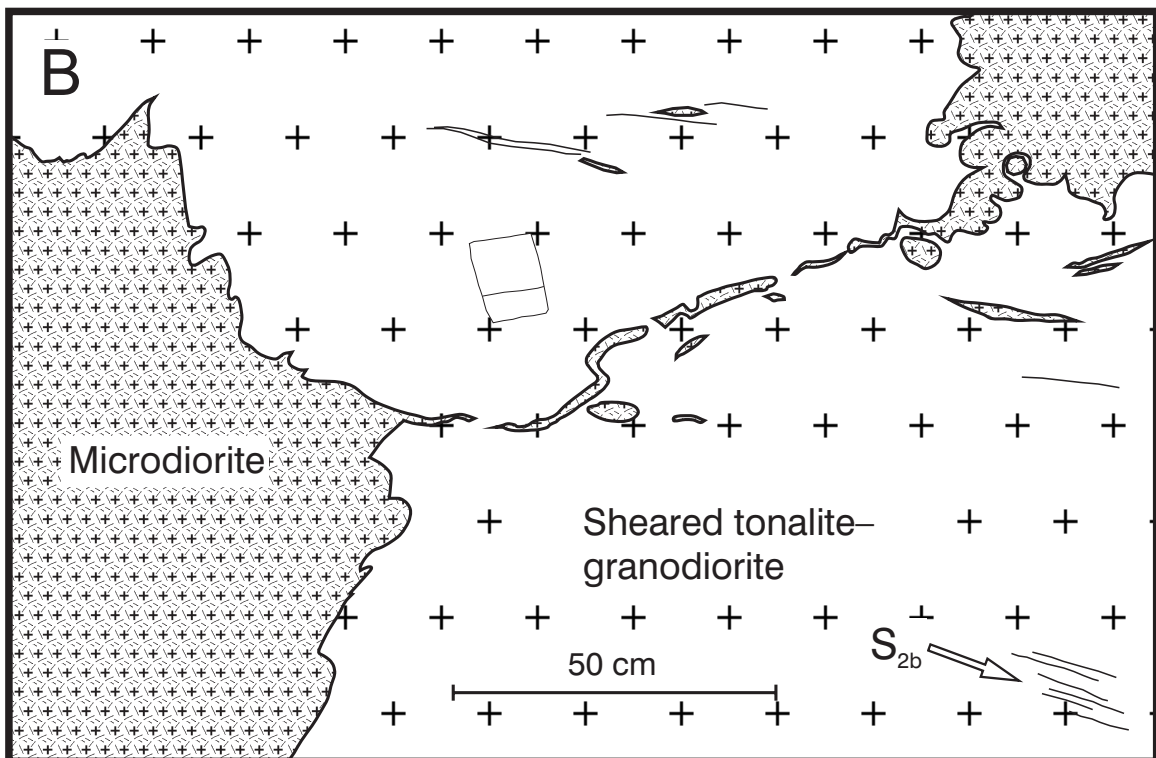
Vaughan, Wareham and Millar, Figure 8



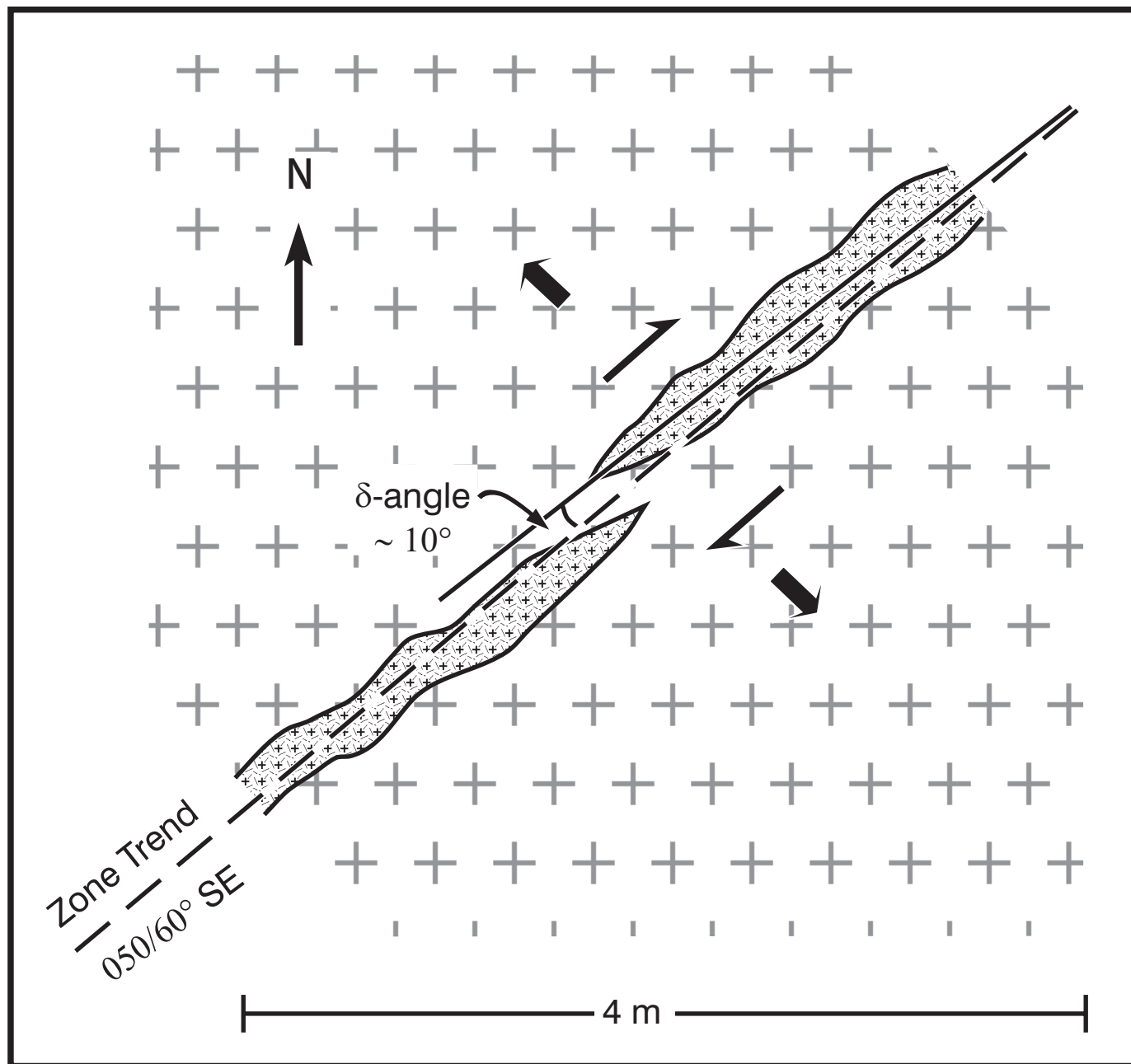
Vaughan, Wareham and Millar, Figure 9

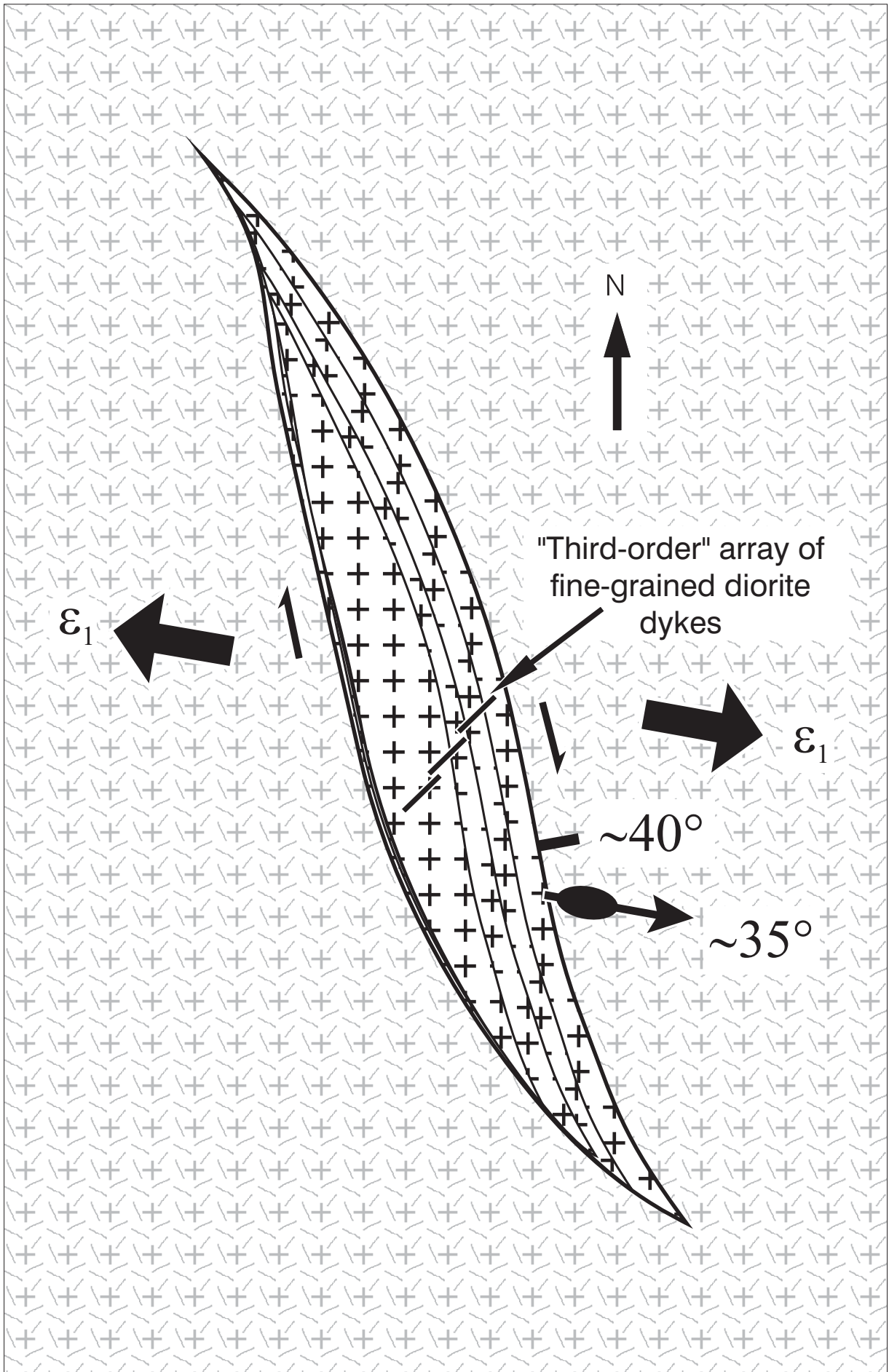


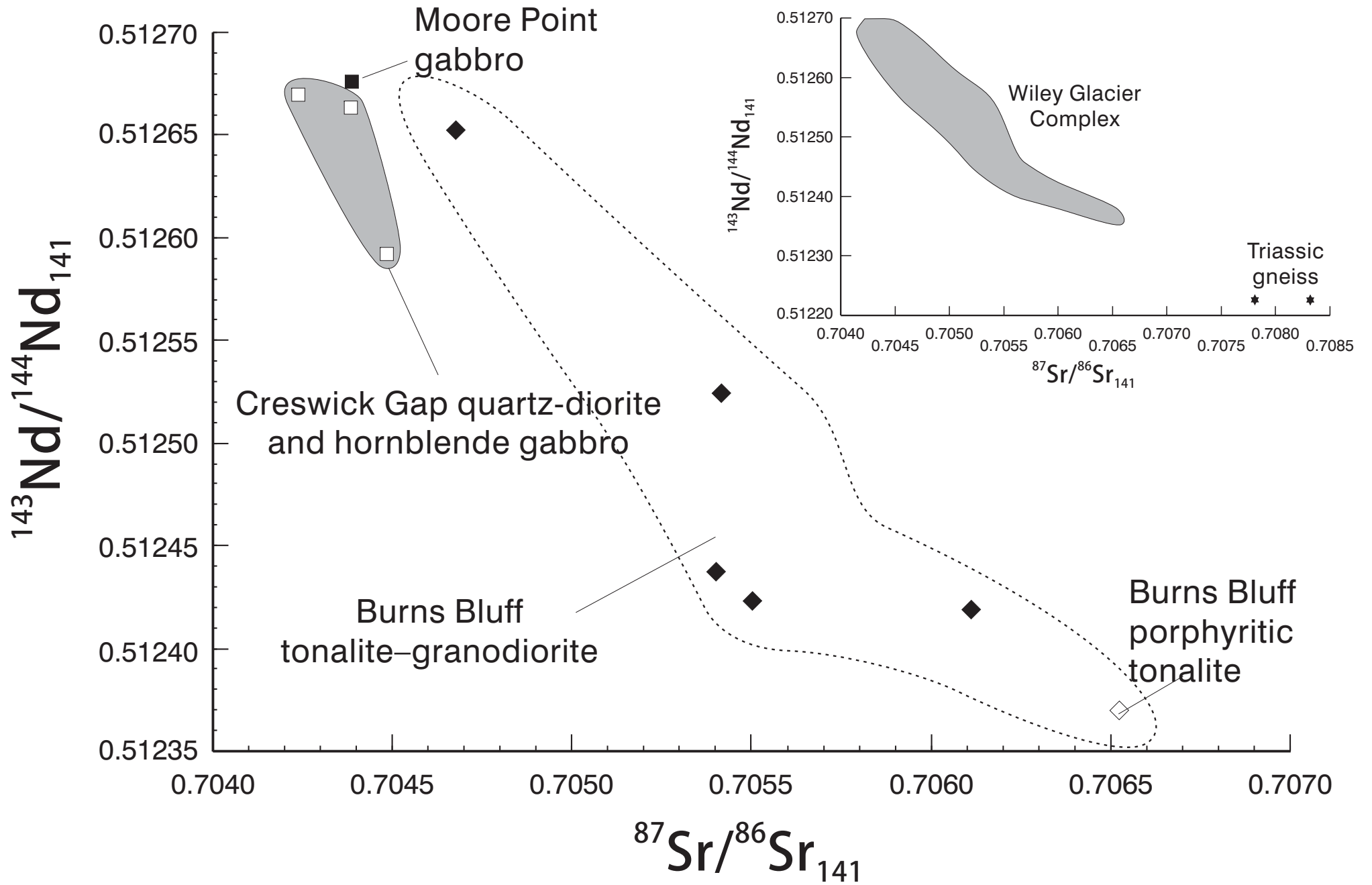
Vaughan, Wareham and Millar, Figure 10



Vaughan, Wareham and Millar, Figure 11



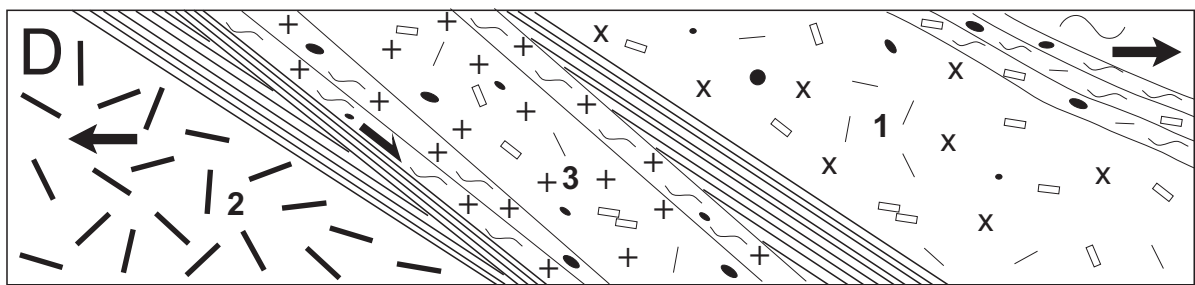
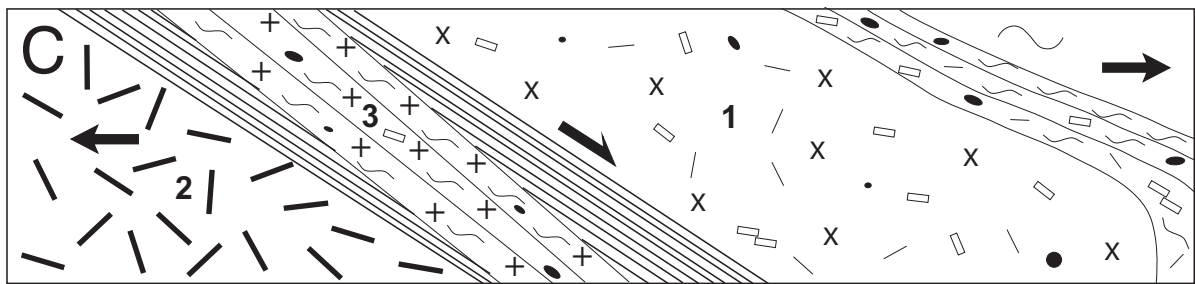
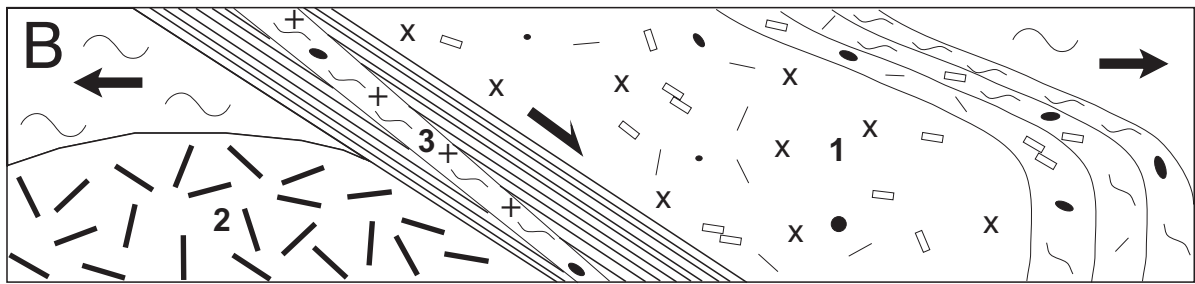
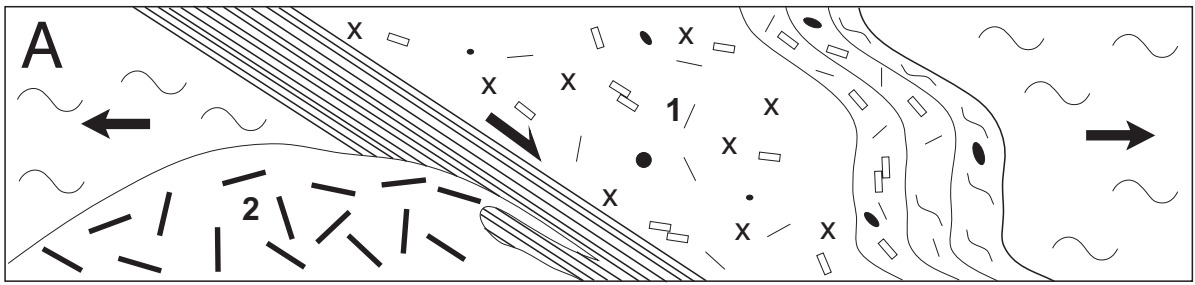




W

Section views

E



Vaughan, Wareham and Millar, Figure 15

